Identification of Soil Arsenic Contamination in Rice Paddy Field Based on Hyperspectral Reflectance Approach

Arnab Saha [1], Bhaskar Sen Gupta [1,*], Sandhya Patidar [1] and Nadia Martínez-Villegas [2]

[1] Institute of Infrastructure and Environment, School of Energy, Geoscience, Infrastructure and Society, Heriot-Watt University, Edinburgh EH14 4AS, UK; as2059@hw.ac.uk (A.S.); s.patidar@hw.ac.uk (S.P.)

[2] Applied Geosciences Department, IPICyT, San Luis Potosi 78216, Mexico; nadia.martinez@ipicyt.edu.mx

* Correspondence: b.sengupta@hw.ac.uk

Abstract: Toxic heavy metals in soil negatively impact soil's physical, biological, and chemical characteristics, and also human wellbeing. The traditional approach of chemical analysis procedures for assessing soil toxicant element concentration is time-consuming and expensive. Due to accessibility, reliability, and rapidity at a high temporal and spatial resolution, hyperspectral remote sensing within the Vis-NIR region is an indispensable and widely used approach in today's world for monitoring broad regions and controlling soil arsenic (As) pollution in agricultural land. This study investigates the effectiveness of hyperspectral reflectance approaches in different regions for assessing soil As pollutants, as well as a basic review of space-borne earth observation hyperspectral sensors. Multivariate and various regression models were developed to avoid collinearity and improve prediction capabilities using spectral bands with the perfect correlation coefficients to access the soil As contamination in previous studies. This review highlights some of the most significant factors to consider when developing a remote sensing approach for soil As contamination in the future, as well as the potential limits of employing spectroscopy data.

Keywords: hyperspectral remote sensing; soil As contamination; rice paddy; spectral analysis

1. Introduction of Arsenic Contaminations

Arsenic (As) is a common element that ranks 20th in abundance in the earth's crust, 14th in seawater, and 12th in the human body [1,2]. As makes up about 0.00005% of the earth's crust [3], with an average concentration of 2.0 mg·kg^{-1} in igneous and sedimentary rocks. It varies from 0.5 to 2.5 mg·kg^{-1} in most minerals [4], with higher concentrations in finer-grained argillaceous sediments and phosphorites [2]. As is found in over 200 different mineral types in nature, with arsenates accounting for roughly 60%, sulphides and sulfosalts for 20%, and arsenides, arsenites, oxides, silicates, and elemental As accounting for the remaining 20% [5]. As is present in different forms of metalliferous deposits in its most recoverable form. Arsenopyrite is the most abundant As mineral [2]. Soils have higher levels of As than minerals [6]. Uncontaminated soils typically contain 1–40 mg·kg^{-1} As, with the lowest concentrations in sandy soils and those originating from granites and the highest concentrations in alluvial and organic soils [4]. Even though As is ubiquitous on the Earth's surface, long-term interaction with high levels of As can be harmful to human health [7,8].

Rice is consumed by half of the global population every day, rendering it a significant source of nutrition for billions of humans. Rice may contain As, which is harmful to human health, depending on the way it is grown [9,10]. As is a poisonous nonessential metalloid found in high concentrations in rice grains in some parts of the world, posing a serious threat to rice yield and quality. As a result, the rice–As interactions have been extensively studied over the last few decades. Rice is responsible for 60% of human As toxicity in the Chinese population [11]. If we can solve the As accumulation problem in

rice, we should be able to reduce As-related diseases in the affected areas. Such diseases are prevalent in South and Southeast Asia, including Bangladesh and some Indian states [12]. A detailed understanding of the factors that affect the assimilation and translocation of As from the soil to grains can be useful in addressing this problem and lowering crop As levels. Rice plant uptake at the root surface is affected by factors such as iron plaque and radial oxygen loss [13]. Rice contamination is not just a concern in Asia. The Consumers Union, a consumer advocate organisation headquartered in the United States, reported alarming levels of As in rice sold in the United States in a 2012 survey.

The world average As concentration in soils is estimated to be around 5–7.5 mg/kg [14,15]. A regulatory limit of 0.2–0.4 mg/kg As in rice is suggested by the United Nations World Health Organization [10]. Rice grains have been found to have levels as high as 1.8 mg/kg in previous research [16]. These amounts of As can lead to potentially harmful exposure to humans and animals, which may cause life-threatening complications [17]. Pinson et al., (2015) [18] analysed around 1763 rice strains from around the world. They reported that certain American rice varieties had slightly lower As concentrations than other rice varieties cultivated in the same environment. As concentration prediction accuracy is essential for food safety and precision farming. Carbonell-Barrachina et al., 2009 [19] opined that the amount of total and inorganic As (t-As and i-As) consumed was dependent on the nature of drinking and cooking water, as well as the amount of seafood and rice consumed. The key issues arise in countries with low water quality, where the population relies on rice for survival. Considering the health risks associated with As in rice, considerable efforts have been made to assess As pollution in paddy soils [20–23] and establish preventive strategies to minimise As uptake by rice plants [24–27]. Field sampling accompanied by wet chemistry methods and interpolation approaches is a popular way of detecting As contamination, but it is time-consuming and costly [28,29]. Furthermore, as prevention methods (e.g., silicon fertilisation) are used to regulate As absorption into plant sections, it is essential to track the level of reductions periodically to ensure that As accumulation is fully remedied. The use of field sampling and wet chemistry methods for routine monitoring of As absorption at large scales is extremely difficult [30]. Meharg and Rahman (2003) [16] reported the findings of an As survey of paddy soils obtained for a wide region of Bangladesh.

As can be found in a wide variety of chemical forms in the environment, with arsenate (As(V)) and arsenite (As(III)) being the most common and dangerous inorganic forms. Arsenate, as a phosphate analogue, interacts with phosphate metabolism (phosphorylation and ATP synthesis) in plants, whereas As(III) relates to sulfhydryl protein molecules, affecting their structures and/or electrochemical functions [31,32]. Plants exposed to high concentrations of As suffer from oxidative stress, which has a direct impact on metabolic activities such as cell division and photosynthetic activity [33–35]. As concentration in rice plants has been linked to low sensitivity in chlorophyll content, crippled plant growth, and chlorotic side effects; plants that show these symptoms are commonly referred to as stressed plants according to recent research [36–38].

The authors of this paper have reviewed the current information and evidence on hyperspectral remote sensing approaches for soil As contamination measurement in rice paddy fields. This paper also discusses how hyperspectral remote sensing sensors and spectroradiometers might be used to assess As pollution in agricultural soils. Figure 1 shows the As cycle of the environment as well as the conceptual framework for identifying the soil As contamination in rice paddy fields using the hyperspectral reflectance approach. The As cycle is a biogeochemical cycle in which As is exchanged naturally and anthropogenically via soil, the lithosphere, ocean, inland water, and the atmosphere.
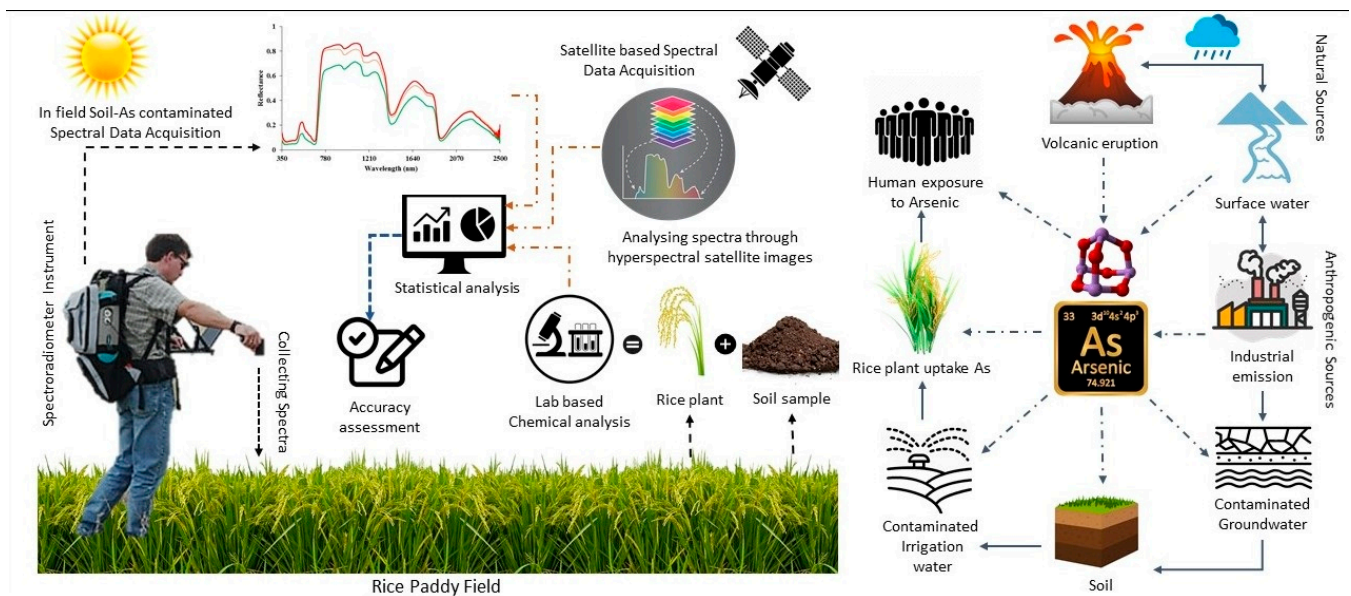
Figure 1. Arsenic cycle of environment and graphical methodology to identify the soil As concentration based on hyperspectral reflectance techniques.

2. Arsenic Concentration in Rice Plants

The quantity of As in a plant is mostly influenced by how much As it is exposed to. Its concentration ranges from less than 0.01 to around 5 μg/g [39]. The physicochemical and biological characteristics of soils are affected by As contamination, resulting in relatively low crop yields [40,41].

Groundwater polluted with As is not only used for drinking but also for irrigating crops, including the staple paddy rice (Oryza sativa). If As levels rise in paddy soils, more As would translocate to rice grains, increasing As exposure from food. Through biochemical reactions such as oxidation and reduction activities, soil microorganisms help the detoxification of hazardous chemicals such as As [42]. Rice is a semi-aquatic plant with widespread aerenchyma in its roots, analogous to wetlands species. This aerenchyma causes O_2 to be infiltrated from the shoots for root respiration. To deal with anaerobic conditions in underwater soil, rice roots' aerenchyma releases some O_2 to the rhizosphere [43]. The rhizosphere is a small area of soil or substrate that is specifically affected by root secretions and related soil microorganisms, also known as the root microbiome [44].

According to the study by Santra et al., 2013 [45], the highest levels of As concentration in soil were found in Bangladesh and parts of West Bengal, India, as shown in Table 1. The highest concentrations of As have also been found in these two places. Figure 2 shows a flowchart that describes how the soil samples are collected and subsequent steps for the identification of As content in agricultural soil.

Table 1. Concentrations of As in soil, crops, and vegetables cultivated in West Bengal, India, and neighbouring countries (adapted from Santra et al., 2013 [45]).

Country	As in Soil (mg/kg)	As in Crops and Vegetables (mg/kg)		References
		Rice	Vegetables	
Bangladesh	NA	0.358	0.034	[46]
West Bengal, India	11.35	0.245	<0.0004–0.693	[47]
Bangladesh	NA	NA	0.306–0.489	[48]
Bangladesh	NA	NA	0.011–0.103	[49]
Bangladesh	7.31–27.28	0.04–0.27	0.2–3.99	[50]

Table 1. *Cont.*

| Country | As in Soil (mg/kg) | As in Crops and Vegetables (mg/kg) | | References |
		Rice	Vegetables	
West Bengal, India	7.0–38.0	0.30	NA	[51]
China	6.04	0.117	0.003–0.116	[52]
Bangladesh	14.5	0.5–0.8	NA	[35]
Nepal	6.1–16.7	0.180	<0.010–0.550	[53]
West Bengal, India	1.34–14.09	0.16–0.58	NA	[54]
West Bengal, India	5.70–9.71	0.334–0.451	0.030–0.654	[55]
Bihar, India	0.027	0.019	0.011–0.015	[56]
West Bengal, India	NA	0.156–0.194	0.069–0.78	[57]
West Bengal, India	NA	0.01–0.64	0.03–0.35	[58]
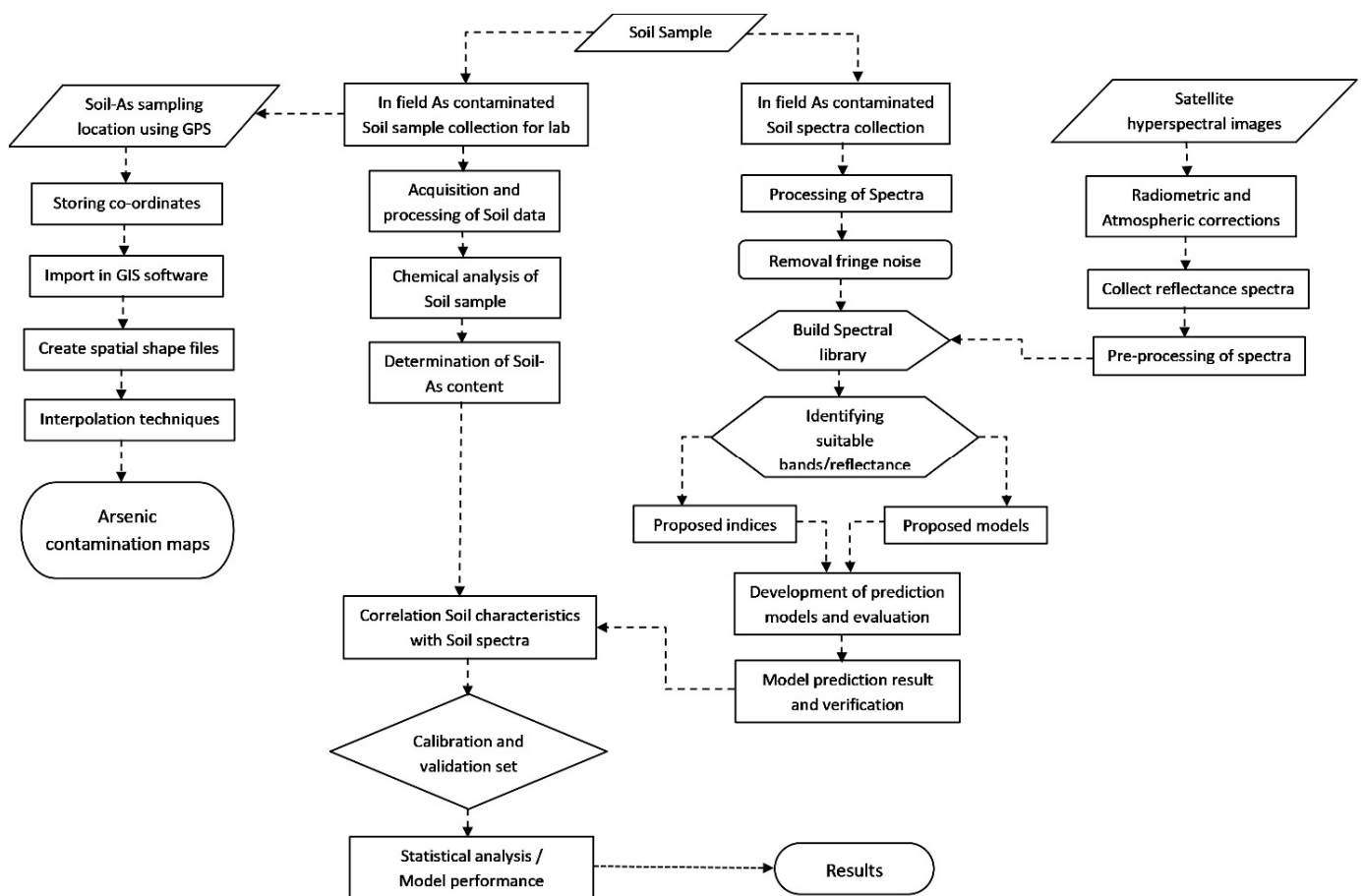
Figure 2. Flowchart for identification of As content in agricultural soil.

3. Use of Remote Sensing

Spectral remote sensing is a valuable technology for estimating agricultural reproduction, crop growth, and physical and biological characteristics in a nondestructive manner [59]. For measuring soil As or heavy metal concentrations, remote sensing techniques offer a low-cost, time-efficient, and environmentally acceptable option, as established by multiple research studies [60–64]. The majority of these studies have focused on relating biophysical factors [65,66], leaf biochemical properties [67,68], moisture content [69–71], and plant stress [72,73] to the spectral response of plants. Hyperspectral remote sensing has been widely used in plant research and agricultural crop management to measure and track plant stress caused by a variety of factors, e.g., nutrient and water deficiency, diseases,

and metal accumulation [74–76]. Plant spectral properties (reflectance and transmittance) at specific wavelengths are affected by changes in leaf biochemical contents (e.g., chlorophyll) caused by stress [77]. Predictive models have been constructed using these changes to determine plant stress using various statistical approaches (e.g., linear regression, partial least squares regression, and random forests). Extraneous factors, such as soil context background reflectance, often confound spectral response to the dependent variable; consequently, two or more bands are used to produce vegetative indices (VIs) using ratios, slopes, or other formulations to minimise their effects [78–80]. The performance of the VIs varies depending on how resistant they are to parameters such as leaf area per unit ground surface area (LAI) and soil context reflectance. As a result, when choosing VI, it is critical to consider the VIs' vulnerability to variations in plant stress along with their resistance to external influences [81].

Artificial neural networks (ANN), support vector machines (SVM), and random forests (RF) are examples of machine learning approaches that could map nonlinear spectral responses of plants under heavy metal stress. Random forests, a new expansion of decision tree learning, is often proposed. In several implementations, random forests have outperformed other machine learning methods in terms of estimation and classification [82,83].

3.1. Hyperspectral Reflectance Measurement

For environmental monitoring and mapping of different heavy metal soil pollutants, hyperspectral remote sensing has been acknowledged as an efficient and noncontact detection approach [61,84]. Soil biochemical parameters (including pH, mineral composition, and microbial activity) have no impact on utilising hyperspectral data to evaluate As and heavy metal concentrations in agricultural soil [85]. In the study by Carter, 1993 [73], leaf spectral reflectances were evaluated to see whether plant stress responses differed depending on the source of stress and the species. Reflectance at visible wavelengths improved in stressed leaves from vascular plant species as a result of reduced pigment absorption. The wavelength ranges of 535–640 nm and 685–700 nm are the most vulnerable to stress in visible reflectance. Near 670 nm, a sensitivity minimum was consistently observed. Infrared reflectance was relatively unaffected by stress but increased at 1400–2500 nm in response to extreme leaf dehydration and reduced water content. As a result, visible reflectance, rather than infrared reflectance, proved to be the most accurate measure of plant stress. The fact that visible reflectance responses to stress were not specific for each stress factor lends credence to the idea that plant physiological responses to stress are identical regardless of the source of stress [86]. Visible near-infrared diffuse reflectance spectroscopy (VisNIR-DRS) is fast becoming a usable, rapid, and noninvasive tool for characterising multiple soil properties simultaneously from reflectance spectra [87].

Spectral Data Pretreatments

These are commonly used spectral pretreatment methods which are described in various research articles, as shown in Table 2.

Table 2. Various spectral pretreatment methods with descriptions.

Spectral Pretreatment Methods	Descriptions	References
Baseline correction (BC)	The most widely used spectral pretreatment approach in NIR. This approach removes the significance of the lowest level in the spectral range from all of the variables in each sampling and has been applied to smoothing and resampling reflectance spectra.	[88,89]

Table 2. *Cont.*

Spectral Pretreatment Methods	Descriptions	References
Standard normal variate (SNV)	A row-oriented spectral treatment that centres and scales each wavelength to reduce dispersion effects. In this method, by splitting the spectral standard deviation and removing the spectral mean, each spectrum is transformed.	[89,90]
Multiplicative scatter correction (MSC)	A spectral data processing approach that corrects the multiplicative and cumulative dispersion effects. SNV and MSC are the same functional criteria, but the main difference is SNV is used for individual spectral reflectance, whereas MSC has been applied for reference spectral reflectance.	[89,91,92]
First and second derivation (FD and SD)	These significantly reduce background influences and improve spectral data inflexion characteristics and spectral overlapping.	[92]
Continuum removal (CR)	This creates additional spectral information by splitting a continuum's envelope curve on unprocessed reflectance spectra to develop new reflectance spectra.	[93]
Savitzky–Golay (SG) smoothing	Applied to the pretreatment of spectra, this is a common smoothness filtering method. It is a low-pass filter that smooths spectra by removing high-frequency noise while allowing low-frequency signals to pass through. Before evaluating the FD and SD, SG smoothing is performed.	[92,94]
log(1/R)	This is one of the most common spectral pretreatment transformation methods, where reflectance (R) enacts linearisation between the spectra and heavy metal content in soil by highlighting the edges of absorption bands.	[79,92]

In the study by Chakraborty et al., 2017 [95], soil absorption wavelengths S1 and S2, with the lowest (2.42 mg/kg) and highest (10.37 mg/kg) t-As concentrations as a result of t-As heterogeneity, were depicted using continuum-removed spectra to contrast individual absorption features against a standard baseline, as shown in Figure 3. The high optical intensity or absorption spectrum in the visible range (350–750 nm) and specific absorptions near 1400, 1900, and 2200 nm seemed to be similar for both soils. Continuum removal is used to normalise reflectance spectra so that individual absorption features can be compared against a standard baseline. The continuum is a convex framework that fits over the top of a spectrum and connects local spectra peak values using straight-line segments. The continuum is removed by dividing it into the specific spectrum for each pixel in the image using Equation (1) [96].

$$S_{cr} = S/C \tag{1}$$

S_{cr} = Continuum-removed spectra
S = Original spectrum
C = Continuum curve

where the continuum and spectra align and the first and last bands in the output continuum-removed data file are equal to 1.0, and where absorption features occur, they are less than 1.0.
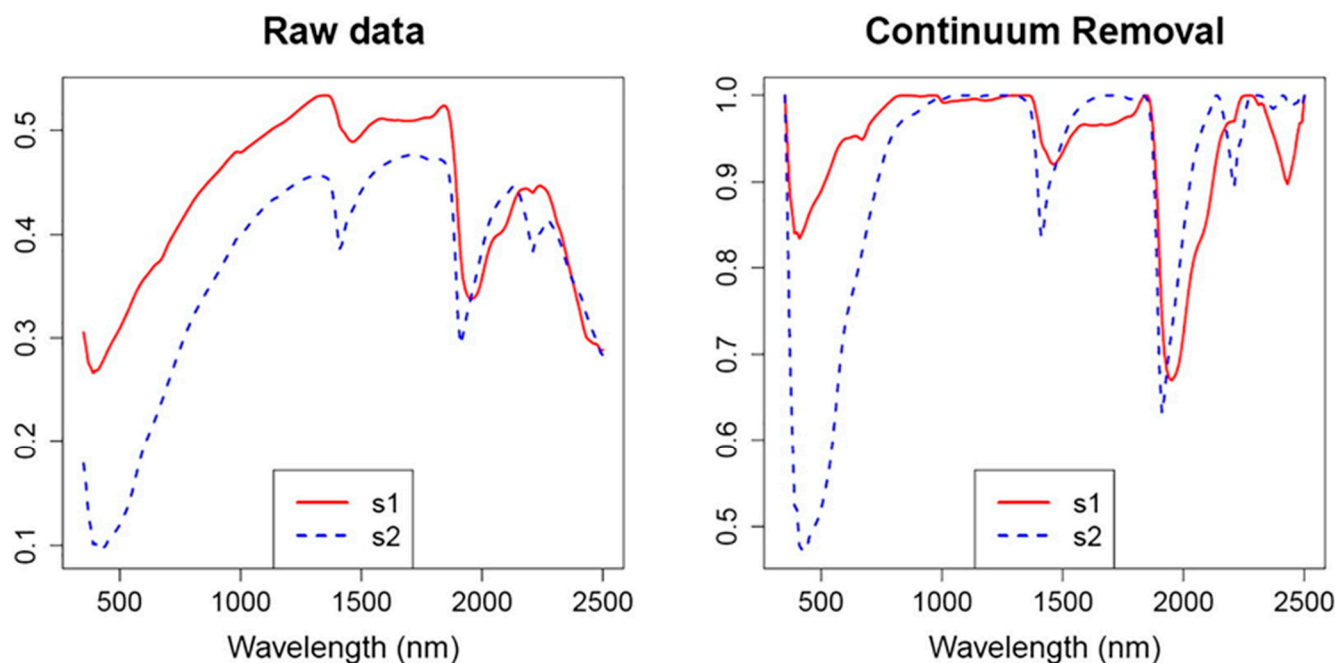
Raw data   **Continuum Removal**

Figure 3. Plots of the typical reflectance spectra and continuum-removed spectra of the two different types of soils with the lowest (S1) and highest (S2) total As contents (adapted from Chakraborty et al., 2017 [95]).

3.2. Spectra Collection

In the previous study, canopy reflectance spectra were collected from rice using an Analytical Spectral Device (ASD) FieldSpec 3 spectrometer, which has a spectral range between 350 and 2500 nm with a sampling interval of 1.4 nm in the 350–1000 nm range and 2 nm in the 1000–2500 nm range. With a sensor height of 1 m above rice canopies, the ASD field of view was adjusted to 25°. Both observations were taken at noon between 10:00 a.m. and 2:00 p.m. local time on unclouded clear days. Under the same lighting conditions, a white Spectralon reference panel was used to measure relative reflectance spectra by splitting leaf radiance by the reference radiance for each wavelength. At each point, ten scans were taken and combined to create a single spectrum. A total of 60 spectral measurements were taken [82].

In the research of Chakraborty et al., 2017 [95], a portable visible NIR spectroradiometer PSR-3500® was used to measure the spectral reflectance of air-dried and finely ground (b200 m) soil samples proximally over the VisNIR field (350–2500 nm). The performance values of the reflectance data became quantised to 10 nm, and the scanning was performed using a touch probe with a 5 W halogen lamp, which reduced stray light errors. In this research, the essential spline fitting function of Chakraborty et al., 2014 [97] was used in R 2.11.0, the statistical computing open-source software (R: The R Project for Statistical Computing [98]) to handle raw standard reflectance spectra. To create the As prediction model, they used three different spectral preprocessing methods, i.e., Savitzky–Golay 1D, 2D, and orthogonal signal correction (OSC); one of these, the Savitzky–Golay 1D method, was taken from Luo et al., 2005 [99].

Figure 4 depicts the curves of various spectral preprocessing approaches as reported by Han et al., 2020 [100]. A FieldSpec 4 field spectrum analyzer was used to determine the spectral reflectance of the soil samples in a dark room. The experiments were carried out in a dark room with a 50 W halogen lamp located 0.3 m away from the selected samples

and with a zenith angle of 25°. Before obtaining one of the five samples, the device was calibrated using the radiance of a white reflection panel. The reflectance spectrum of the soil samples was measured using the sum of the ten spectral curves for each soil sample. One of the fundamental stages in spectral preprocessing is spectral resampling, which has a significant impact on the hyperspectral prediction model's accuracy. The spectral data were subjected to first derivation (FD), second derivation (SD), and multiplicative scatter correction (MSC) to demonstrate the spectral curves' absorption and reflection characteristics while removing data redundancy between bands. For smoothing spectral curves and improving data quality, the digital filtering Savitzky–Golay (SG) algorithm was used without affecting signal patterns. These spectral transformation approaches were successfully used in hyperspectral soil science research, with positive outcomes [101–103]. The methods, spectral pretreatment processes, algorithms, and results that were discussed in the previous study based on hyperspectral approaches for soil As contamination are summarised in Table 3.
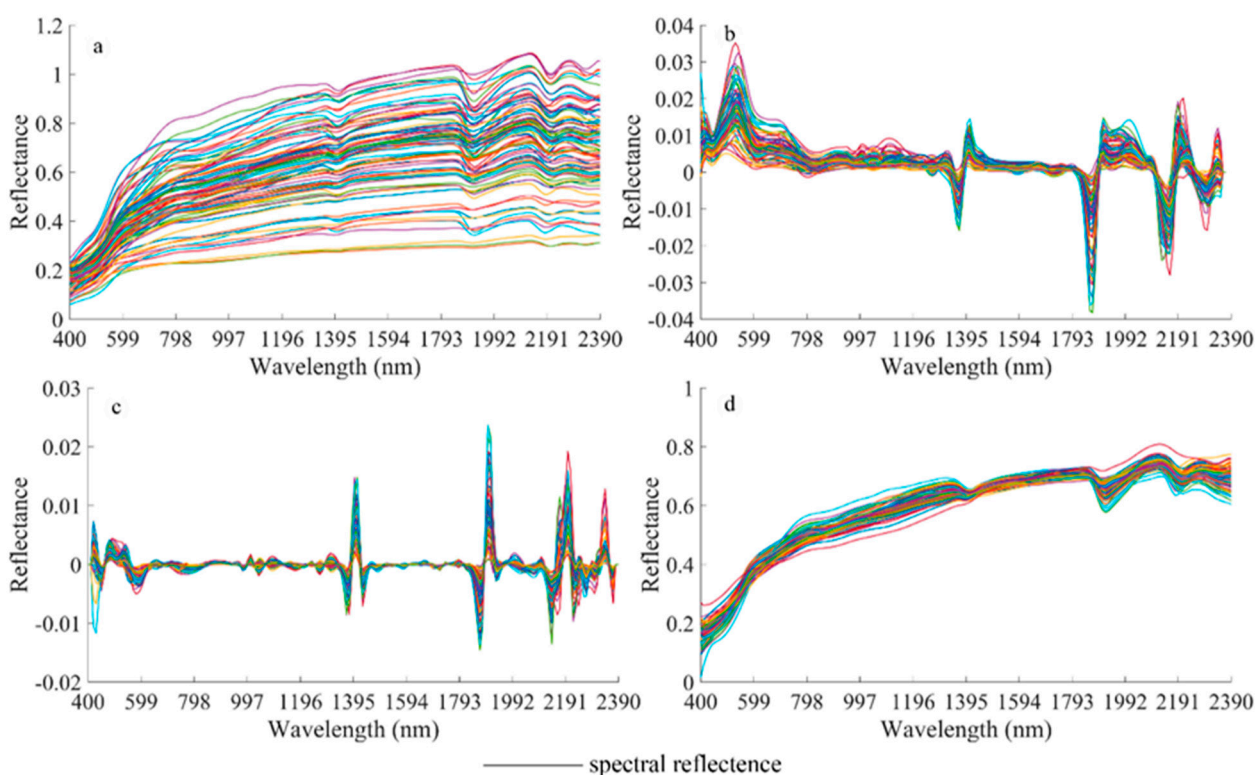

Figure 4. The spectral reflectance of the soil As contaminant samples, (**a**) Savitzky–Golay (SG), (**b**) first derivation (FD), (**c**) second derivation (SD), and (**d**) multiplicative scatter correction (MSC). (Each curve depicts the spectral profile of a single soil sample) (adapted from Han et al., 2020 [100]).

Table 3. Review of hyperspectral reflectance approach in soil As contamination.

Methods	Models' Algorithm	Results	Location	Conclusion	References
Standard Vis-NIR reflectance spectroscopy and indirect—Fe, Fe_2O_3 approach	Multiple linear regression (MLR) and artificial neural network (ANN)	Using MLR-R^2 = 0.837, using ANN-R^2 = 0.858	Near Seville, Spain	Results suggest that by utilising quick and cost-effective reflectance spectroscopy, it is possible to anticipate heavy metals in soils affected by mining residues.	[60]

Methods	Models' Algorithm	Results	Location	Conclusion	References
Standard Vis-NIR reflectance and variations in the spectral absorption features of lattice OH and oxygen on the mineral surface	Pearson correlation coefficient	$R^2 = 0.876$	Rodalquilar gold-mining area, south-eastern Spain	The results suggest that the variables generated from spectral absorption characteristics might be useful in assessing and monitoring As heavy metal concentration.	[61]
Standard Vis-NIR reflectance spectroscopy and indirect Fe_2O_3 approach	Partial least square regression (PLSR)	Root mean square error of cross-validation (RMSEcv) = 1.23 and root mean square error of prediction (RMSEP) = 1.65.	Nanjing area, China	The results suggest that remote sensing data might be used to map As-contaminated areas at a low cost. It is strongly suggested that future research using remote sensing data and field measurements be carried out.	[84]
Vis-NIR hyperspectral reflectance spectroscopy along with FD, SD, and MSC spectral resampling transformation based on the proposed model	Partial least squares regression (PLSR), support vector regression (SVR), and back propagation neural network (BPNN)	Using PLSR-$R^2 = 0.77$, RPD = 1.89 using SVR-$R^2 = 0.72$, RPD = 1.03 using BPNN-$R^2 = 0.86$, RPD = 2.53	Shangluo and Weinan, Shaanxi Province, China	BPNN has the best modelling accuracy, according to the data. In conclusion, estimating soil AS concentration using BPNN and hyperspectral data is possible. The nonlinear issue between soil As concentration and reflectance spectra may be efficiently solved using the BPNN model.	[100]
Standard Vis-NIR reflectance spectroscopy and indirect SOC, Fe_2O_3 approach	Partial least square regression (PLSR)	$R^2 = 0.72$, RMSEP = 0.86, RPD = 1.90	Baguazhou Island, Jiangsu Province, China	Reflectance spectroscopy is a nonanalytical technology that may be used not only to anticipate spectral active components but also trace components that have no spectral features.	[104]
Standard Vis-NIR reflectance spectral absorption feature parameters (SAFPs) and kriging interpolation technique are used as the gridding method for producing measured and predicted As contour maps.	Stepwise multiple linear regression (SMLR) and enter multiple linear regression (EMLR)	Using SMLR-$R^2 = 0.372$, using EMLR-$R^2 = 0.598$	Suncheon, Republic of Korea	The geographic patterns of As concentration contour map based on EMLR-derived values were comparable to those of a map based on observed values, and the EMLR model showed a better qualitative prediction performance than SMLR.	[105]
Diffuse Vis-NIR reflectance spectroscopy and indirect Al_2O_3, Fe_2O_3, TOC approach	Univariate regression	Correlation coefficient (R) = 0.552	Changjiang River Delta, China	This research implies that analysing DRS in the Visible-NIR region could be utilised to derive binding forms and estimate As heavy metal concentrations in agricultural soils.	[106]

Methods	Models' Algorithm	Results	Location	Conclusion	References
Vis-NIR hyperspectral reflectance spectroscopy along with SG, FD, CR, and standard normal variate (SNV) spectral resampling transformation based on hydride generation atomic fluorescence spectrometry (HG-AFS) analysis	Multiple linear regression (MLR), partial least squares regression (PLSR), and adaptive neural fuzzy inference system (ANFIS)	Using MLR-R^2 = 0.87, RMSE = 1.25, using PLSR-R^2 = 0.88, RMSE = 1.22, using ANFIS-R^2 = 0.94, RMSE = 0.88	Liuxin mining area, northwest of Xuzhou, Jiangsu Province, China	In order to improve public health, the ANFIS model and reflectance spectroscopy can map the geographic pattern of soil As concentration.	[107]
Multivariate analysis Using PLSR and SVMR, cross-validation of Vis-NIR diffuse reflectance spectroscopy.	Partial least square regression (PLSR) and support vector machine regression (SVMR)	Using PLSR-Cross Validation (RMSEPcv) = 2.98, maximal coefficient of determination (R^2cv) = 0.61 and residual prediction deviation (RPD) = 1.81, using SVMR-RMSEPcv = 1.89, R^2cv = 0.89 and RPD = 2.63.	Bílina and Tušimice mine areas, Czech Republic	The results show that Vis-NIR reflectance spectroscopy, in combination with the first derivative and SVMR, is a potential technique for soil As monitoring in high-risk areas.	[108]
Lab-based and field-based reflectance spectroscopy based on iteratively retaining informative variables (IRIV) and iteratively retaining informative variables coupled with Spearman's rank correlation analysis (IRIV-SCA)	Partial least squares regression (PLSR), Bayesian ridge regression (BRR), ridge regression (RR), kernel ridge regression (KRR), support vector machine regression (SVMR), extreme gradient boosting (XGBoost) regression, and random forest regression (RFR)	Best model results are showing here- **IRIV approach**, for lab spectra (Bayesian ridge regression (BRR)-R^2 = 0.79, RMSE = 0.44, MAE (mean absolute error) = 0.36 for field spectra (random forest regression (RFR))-R^2 = 0.49, RMSE = 0.67, MAE = 0.56. **IRIV-SCA approach**, For lab spectra (support vector machine regression (SVMR))-R^2 = 0.97, RMSE = 0.22, MAE = 0.11, for field spectra (extreme gradient boosting (XGBoost))-R^2 = 0.83, RMSE = 0.35, MAE = 0.29.	Daye city area of the Jianghan Plain region, the southeast of Hubei Province, China	The suggested approach considerably enhances the effectiveness and consistency of the inversion of soil As concentration, and it may be utilised for reliable data for decision making for the remediation and restoration of As pollution across a vast region.	[109]

Table 3. *Cont.*

Methods	Models' Algorithm	Results	Location	Conclusion	References
Vis-NIR reflectance spectroscopy based on the traditional modelling method and transfer component analysis (TCA)	Partial least squares regression (PLSR)	Using the **traditional modelling method**— In first pair of study areas—$R^2 = 0.02$, RPD = 0.65, in the second pair of study areas—$R^2 = 0.01$, RPD = 1.0.1, using **transfer component analysis (TCA)** method— in first pair of study areas—$R^2 = 0.68$, RPD = 1.54, in the second pair of study areas—$R^2 = 0.64$, RPD = 1.66	First pair of study areas—Yuanping in Shanxi Province and Baoding in Hebei Province, China. Second pair of study areas—Chenzhou and Hengyang, located in Hunan Province, China	The findings show that developing future implementations of transferable spectroscopic diagnostic models for predicting soil As concentrations in vast areas at a cheaper cost is a possible path forward.	[110]
Vis-NIR reflectance spectroscopy and CNN model with convolutional autoencoder as a deep learning method	Convolutional neural network (CNN), artificial neural network (ANN), and random forest regression (RFR)	Using CNN-$R^2 = 0.82$, RMSE = 0.359, using ANN-$R^2 = 0.63$, RMSE = 0.725, using RFR-$R^2 = 0.64$, RMSE = 0.564	Geum River watershed of South Korea, Republic of Korea	Deep learning algorithms can estimate As concentrations in soil, according to this study and the CNN-model-acquired robust characteristics from the convolutional autoencoder, which disentangled the key characteristics of several heavy metal elements and generated generally accurate estimations.	[111]
Hyperspectral reflectance spectroscopy based on the stable competitive adaptive reweighting sampling algorithm (sCARS) and sCARS coupled with the successive projections algorithm (sCARS-SPA) approach	Partial least squares regression (PLSR), radial basis function neural network (RBFNN), and shuffled frog leaping algorithm optimization of the RBFNN (SFLA-RBFNN)	Best model results are shown here- **sCARS algorithm**: for Honghu area—SFLA-RBFNN model-$R^2 = 0.85$, RMSE = 0.96, MAE = 0.78 for Daye area—SFLA-RBFNN model-$R^2 = 0.84$, RMSE = 0.30, MAE = 0.25 **sCARS-SPA algorithm**, for Honghu area—SFLA-RBFNN model-$R^2 = 0.88$, RMSE = 0.85, MAE = 0.72 for Daye area—SFLA-RBFNN model-$R^2 = 0.93$, RMSE = 0.22, MAE = 0.17	Honghu and Daye, Hubei Province, China	The findings of the study suggest that the sCARS-SPA-SFLA-RBFNN model may be used to analyse the As concentration of soil. The model not only minimises spectral redundancy and eliminates collinearity, but it also has a better prediction performance. It gives a mechanism for predicting soil As concentration on a broad scale with great accuracy.	[112]

4. Methods for Arsenic Measurement

4.1. Hydroponic Method for Evaluating Leaf and Canopy Reflectance of Stressed Rice Plants for As Contaminants

The feasibility of using reflectance spectroscopy to monitor As in rice plants was investigated by Bandaru et al., 2016 [30] with the application of 0, 5, 10, and 20 μmol As·L^{-1}

sodium arsenate (Na_2HAsO_4) to hydroponically grown rice plants. This study examined whether spectral characteristics could be used to monitor As levels in paddy rice crops. The hydroponic experiments were conducted in an aerated standing nutrient solution [113]. The reflectance spectra of the upper extended leaves were measured in visible and near-infrared (NIR) wavelengths. Alternatively, the SAIL model (scattering by arbitrarily inclined leaves) was used to simulate canopy reflectance for the four As levels for different soil moisture conditions and leaf area indices (LAI). Consequently, the susceptibility of different vegetative indices (VIs) to As concentrations was investigated. Several measurement techniques have been reported, such as (i) leaf spectral measurements, (ii) biophysicochemical measurements, (iii) soil reflectance measurements, (iv) simulated canopy reflectance, and (v) analysis of many vegetation indices evaluated for prediction of As concentration (NDVI—normalized difference vegetation index [114], (vi) OSAVI—optimized soil adjusted vegetation index [115], (viii) MCARI—modified chlorophyll absorption reflectance index [80], (ix) TCARI—transformed chlorophyll absorption reflectance index [30,116], and (x) PDR—peaks derivative ratio [117]. Other abiotic (e.g., ambient noise) and biotic (e.g., pest damage) factors confound reflectance characteristics in the field, so these relationships should be tested using field data. As-induced plant stress cause major variations in leaf spectral characteristics, which could help in monitoring As levels in rice using spectroscopic analysis.

4.2. Estimation of Soil As Using Generated Model and Hyperspectral Remote Sensing

Wei et al., 2020 [112] suggested that heavy metal concentration in the soil can be effectively monitored using hyperspectral remote sensing. Considering the potential for a dynamic nonlinear interaction between soil As content and the spectrum, as well as data redundancy, a reliable model is urgently required. In Daye and Honghu (Hubei Province, China), 62 and 27 samples were collected from two locations in response to this requirement. The soil As material was calculated using hyperspectral data and the two characteristic selection methods of sCARS (stable competitive adaptive reweighting sampling algorithm) [118,119] and sCARS-SPA (the sCARS coupled with the successive projections algorithm) [120]. Furthermore, the three modelling methods of PLSR (partial least squares regression) [121], RBFNN (radial basis function neural network) [122,123], and SFLA-RBFNN (shuffled frog-leaping algorithm optimization of the RBFNN) were also used for the algorithm. The As content and spectral reflectance were determined in the laboratory by spectral calculation as well as through physical and chemical analyses. After completing the continuum removal (CR), the stability competitive adaptive reweighting sampling algorithm coupled with the successive projections algorithm (sCARS-SPA) was used to identify characteristic bands, effectively resolving the issue of data consistency and collinearity. The findings of the experiment show that the sCARS-SPA-SFLA-RBFNN model can be used to analyse the spectral quality of soil As. The model not only decreases spectral information redundancy and removes collinearity, but also has a high prediction accuracy. It provides a tool for forecasting soil As material on a broad scale with high precision.

Wei et al., 2019, in another study [109], examined soil As content for the transferability of the prediction method using laboratory and field reflectance spectroscopy. More than 60 soil samples were obtained for this research, which was focused on spectral analysis of soil samples in the lab as well as in the field using hyperspectral techniques, as shown in Figure 5. The SVC HR-1024 field spectrometer was used to measure the spectra of the soil during the field spectral measurement stage (Figure 5b). Field spectral measurements were taken on a sunny day at noon to maintain a proper solar altitude angle, and the probe's field of view angle was 25 degrees. The spectra of the soil samples were measured in the laboratory using an ASD FieldSpec 3 field spectrometer with a spectral resolution of 1 nm (Figure 5a). A 1000 W halogen lamp with a 25-degree field of view and a 15-degree irradiation vertical direction angle was used as the light source around 30 cm from the surface of the soil sample. Before the measurement, both spectrometers were calibrated on a whiteboard for field or lab measurement.
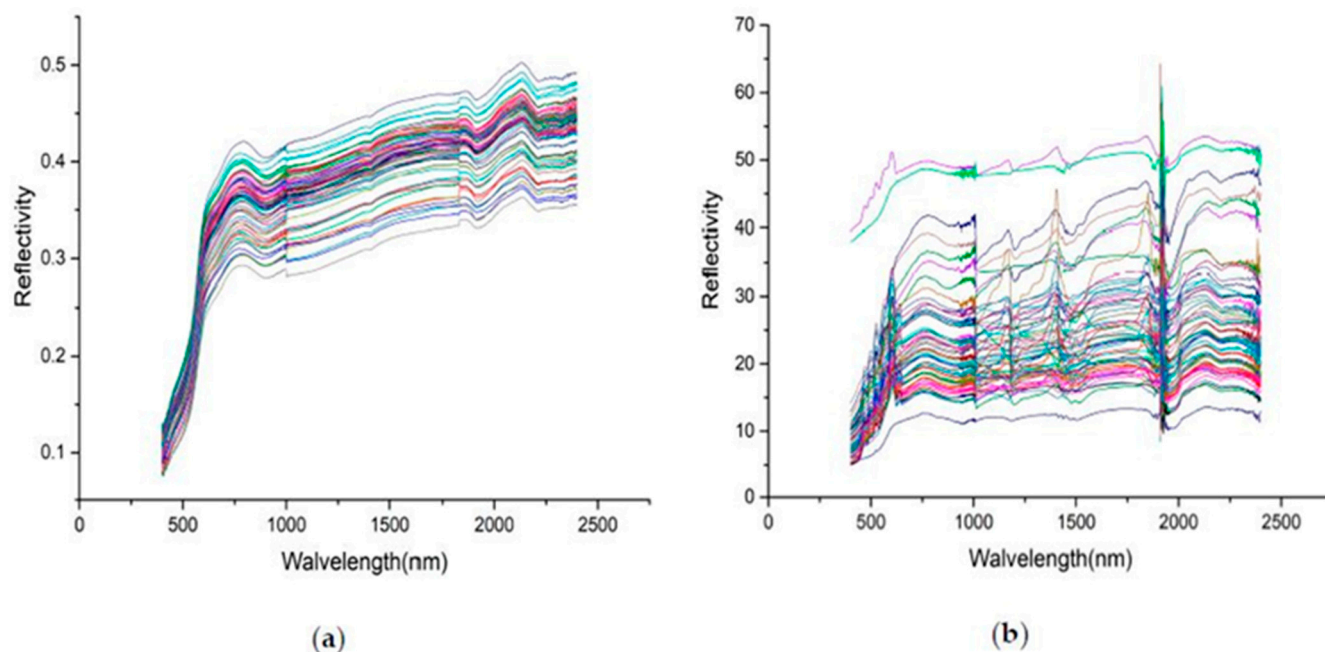
Figure 5. Soil reflectance spectra used to estimate the soil As concentration: (**a**) reflectance spectra in the lab; (**b**) reflectance spectra in the field (adapted from Wei et al., 2019 [109]).

Seven different simulation techniques, namely, (i) PLSR (partial least squares regression) [124], (ii) BRR (Bayesian ridge regression) [125,126], (iii) RR (ridge regression) [127], (iv) KRR (kernel ridge regression) [128], (v) SVMR (support vector machine regression) [129,130], (vi) XGBoost (extreme gradient boosting regression) [131], and (vii) RFR (random forest regression) [132,133], were used based on the two different methods of choosing characteristic bands' IRIV (iteratively retaining informative variables) and IRIV-SCA (IRIV coupled with Spearman's rank correlation analysis) [134,135]. The soil was not air-dried, sieved, ground, or otherwise processed in the field trial, which was more representative of the real-world application scenario. The field-based model's accuracy was lower than the model based on laboratory-measured spectra. The explanation for this is that the natural environment affects the retrieval of measured spectral data; furthermore, the model based on ground spectral data has good stability and actual predictive efficiency, as well as high feasibility. The proposed approach greatly improves the precision and stability of the inversion of soil As material, and it may be used to provide reliable data for decision support for the treatment and recovery of As pollutants over a wide region.

4.3. Visible Near-Infrared Diffuse Reflectance Spectroscopy (VisNIR-DRS) Approach

The VisNIR-DRS method is compact and cost-effective. It also supports high-throughput and can be used in both proximal and remote sensing applications. Typically, a chemometric predictive algorithm is developed using a variety of soil parameters and VisNIR spectral reflectance values. Heavy metals in agricultural soils have also been estimated using the DRS technique [136,137]. In the research of Chakraborty et al., 2017 [95], the VisNIR-DRS spectral data were used to estimate the overall As as well as five separate solid As phases efficiently (Mg, PO_4, O_x, HCl, and org pools). A total of 200 surface soil (0–15 cm) samples were obtained and scanned using VisNIR-DRS from fertile farmland surrounding a contaminated landfill site. For estimating soil t-As, the raw reflectance spectra were preprocessed using three spectral transformations and five extracted pools using partial least squares regression (PLSR). However, the findings are promising, indicating that VisNIR DRS can be used for the analysis of As-polluted soils in the future. It is necessary to investigate its capacity for rapidly screening soil samples for other solid As phases over a larger geographic region.

4.4. Fuzzy Overlay and Spatial Anisotropy Approach

A fuzzy overlay was found to be a useful tool for determining which areas were most likely to be polluted with As at the catchment in Wangsaphung District, Loei Province, in the north-eastern region of Thailand. Traditional overlay analysis applications in geographic information systems (GIS), such as site collection and suitability models, are solved using fuzzy logic. Fuzzy logic is a method of computation that uses "degrees of fact" rather than the standard "true or false" technique (1 or 0). Instead of only determining whether a given value is in or out of a set, a variant on set theory allows specifying the probability that the value is a part of the set [138]. The fuzzy overlay may reveal polluted areas using data sources such as distance to stream, ground slope, and soil permeability. Collection of samples and examination of As content and interpolation surface by spatial anisotropic approach were used to verify high As pollution. A total of 51 soil samples were collected from the polluted site, which was identified using a fuzzy overlay technique. Soil samples were collected at a depth of 0.00–1.00 m from the ground level at each site. The possible high As locations derived from fuzzy overlay outputs were cross-checked from an interpolation surface using the spatial anisotropic method. The spatial surface anisotropic and fuzzy overlay mapping outputs were all spatially conformed in a meaningful way. As a result, the fuzzy overlay has proven to be a simple method for establishing the preliminary site analysis. This tool may be used to detect any heavy metals or polluted materials in water flowing through soil media in general [139].

4.5. Multivariate Hyperspectral Vegetation Indices

For monitoring soil As or heavy metal pollution across wide regions, hyperspectral data are essential. Various research reports have shown that surface-based vegetation indices can be applied to hyperspectral images [61,62,140]. In hyperspectral remote sensing, the green (530–580 nm) and red edge (680–760 nm), as well as the NIR spectral bands, were discovered to be effective for assessing chlorophyll concentration in empirical models. The vegetation indices are used for estimating the chlorophyll content of rice plant leaves or canopies because the chlorophyll in leaves and As concentration in soils have a strong negative correlation [35,141]. In the study by Shi et al., 2016 [142], the canopy reflectance spectra of rice during the transplanting and harvesting period were used to develop different vegetation indices for evaluating As levels in agriculture soils, as shown in Table 4. In Table 4, the published results indicate that the newly developed three-band vegetation index, $(R_{716} - R_{568})/(R_{552} - R_{568})$, performed best in assessing soil As concentrations. This study also revealed that, for soil As contamination monitoring, both two-band and three-band vegetation indices, denoted by PRI (photochemical reflectance index) $(R_{531} - R_{570})/(R_{531} + R_{570})$ and $(R_{762} - R_{732})/(R_{732} - R_{640})$ [141,143] and REP (red-edge position) [144], can be utilised as common vegetation indices. However, according to Shi et al., 2015 [145], three-band vegetation indices may have a greater estimation accuracy than two band indices even though the earlier one uses more appropriate and more informative bands. In the study by Muller, 1969 [146] and Loska et al., 2004 [147], it appeared that the geo-accumulation index (I_{geo}), as shown in Equation (2), could be used to assess the As content in agricultural soils.

$$I_{geo} = \log_2 (C_{As}/1.5B_{As}) \tag{2}$$

where C_{As} is measured As concentration in the soil and B_{As} is the geochemical background value of As.

Table 4. Estimation of soil As concentration using multivariate vegetation indices with the validation results, modified from Shi et al., 2016 [142].

Vegetation Indices		r	RMSE (mg/kg)	References
Two-band vegetation indices	$\{(R_{792} - R_{806})/(R_{792} + R_{806})\} \times 10^3$	0.71	16.24	[142]
	$(R_{792}/R_{806}) \times 10^3$	0.70	16.28	
	$(R_{876} - R_{887}) \times 10^3$	0.63	18.49	
Three-band vegetation indices	$R_{674}/(R_{352} \times R_{526})$	0.33	22.23	
	$\{R_{908}/(R_{860} + R_{930})\} \times 10^2$	0.72	16.18	
	$\{(R_{806} - R_{792})/(R_{806} + R_{770})\} \times 10^3$	0.62	18.45	
	$(R_{716} - R_{568})/(R_{552} - R_{568})$	0.75	15.63	
	$(R_{730} - R_{812})/(R_{730} + R_{812} - 2R_{746})$	0.72	16.17	
Photochemical reflectance index (PRI)	$(R_{531} - R_{570})/(R_{531} + R_{570})$	0.67	17.41	[143,148]
	$(R_{762} - R_{732})/(R_{732} - R_{640})$	0.52	20.89	[141]
	$(D_{752} - D_{711})/(D_{711} - D_{640})$	0.51	21.44	
	$(D_{732} - D_{702})/(D_{732} + D_{702})$	0.57	19.85	
	D_{752}/D_{702}	0.51	21.37	
Red-edge position (REP)	$700 + 40 \left[\{(R_{670} + R_{780})/(2 - R_{700})\}/(R_{740} - R_{700})\right]$ *	0.62	18.65	[144]

* Rn: reflectance value at *n* nm; Dn: the first-derivative reflectance value at *n* nm; the constants 700 and 40 result from interpolation in the 700–740 nm interval.

Table 5 shows the summary of hyperspectral reflectance application in soil As contamination monitoring for rice paddy fields along with As-related plant stress.

Table 5. Review of hyperspectral reflectance approach in soil As contamination of paddy field along with rice plants.

Methods	Model Algorithm	Results	Location	Conclusion	References
Vis-NIR reflectance spectroscopy with various vegetative indices for evaluating leaf and canopy reflectance of stressed rice plants	SAIL (scattering by arbitrarily inclined Leaves)	NDVI-R^2 = 0.69, RMSE = 1.99 OSAVI-R^2 = 0.73, RMSE = 1.84 MCARI-R^2 = 0.85, RMSE = 1.23 TCARI-R^2 = 0.88, RMSE = 1.10 PDR-R^2 = 0.79, RMSE = 1.45 TCARI/OSAVI-R^2 = 0.89, RMSE = 1.11	USDA Beltsville Agricultural Research Facility, Beltsville, MD, USA	The combined index, TCARI/OSAVI, and red-edge-based Vis-MCARI and TCARI showed higher sensitivity to As levels and better resistance to soil backgrounds and LAI.	[30]

Table 5. *Cont.*

Methods	Model Algorithm	Results	Location	Conclusion	References
Lab-based and field-based Vis-NIR reflectance spectroscopy with the data preprocessing methods, Savitzky–Golay smoothing (SG), first derivative (FD), and mean Center (MC) for the spectral pretreatment and normalized difference spectral index (NDSI) approach	Partial least square regression (PLSR)	Using PLSR— for laboratory spectra (FD + SG + MC) — R = 0.64, RMSEP = 14.7 mg/kg, RPD = 1.31, for field spectra (FD + SG + MC) — R = 0.71, RMSEP = 13.7 mg/kg, RPD = 1.43, using NDSI— for field spectra—R = 0.68, RMSEP = 13.7 mg/kg, RPD = 1.36	Zhongxiang, Hubei Province, China	These findings suggest that, by using the reflectance spectra of rice plants, it is possible to detect As contaminants in agricultural soils. The association between As levels in soils and chlorophyll a/b levels and cell structure in rice plant leaves or canopies might be the prediction mechanism. The wavelengths of the spectra at the canopy level around 768, 939, 953, 1132, and 1145 nm are discovered as critical wavelengths for forecasting the As content in agricultural soils.	[79]
Hyperspectral reflectance spectroscopy using random forests	Random forests	$R^2 = 0.84$, MSE = 3.97	Suzhou, Jiangsu Province, China	Hyperspectral remote sensing and random forests are effective ways to quickly estimate As concentrations in rice plants.	[82]
The spectral data pretreatment methods and indirect Fe approach. (First and second derivatives (FD and SD), baseline correction (BC), standard normal variate (SNV), multiplicative scatter correction (MSC), and continuum removal (CR), reused for the spectral reflectance data pretreatments)	Partial least square regression (PLSR)	No spectral pretreatment– RRMSE–0.26, R^2- 0.55, FD-RRMSE–0.24, R^2- 0.61, SD-RRMSE–0.25, R^2- 0.58, CR-RRMSE–0.24, R^2- 0.62, BC-RRMSE–0.25, R^2- 0.59, SNV-RRMSE–0.30, R^2- 0.37, MSC-RRMSE–0.30, R^2- 0.38.	Guiyang suburb on periphery of the Baoshan Mine, southeast Hunan Province, China	In order to build final models, wavebands around 460, 1400, 1900, and 2200 nm are essential spectral variables.	[136]
Proposed three-band hyperspectral vegetation index, normalized difference vegetation index (NDVI), photochemical reflectance index (PRI), and red-edge position (REP) approach	Successive projections algorithm (SPA)	For three-band vegetation index—R = 0.75, RMSE = 15.63 mg/kg, For NDVI–R = 0.71, RMSE = 16.24 mg/kg, For PRI–R = 0.67, RMSE = 17.41 mg/kg, For REP–R = 0.62, RMSE = 18.65 mg/kg	Zhongxiang region of Chinaon, China	The findings suggest that the newly developed proposed three-band vegetation index (R716-R568)/(R552-R568) may be used to estimate the amount of As in the soil in the study region. For monitoring soil, As pollution, PRI and REP may be utilised as universal vegetation indices.	[142]
Diffuse Vis-NIR and MIR reflectance spectroscopy and indirect Al_2O_3, Fe_2O_3, TOC approach	Partial least square regression (PLSR)	$R^2 = 0.455$, RMSEC (root mean square error of calibration) = 1.86, RMSEP (root mean squared error of prediction) = 1.607, RPD = 1.137	Jiangsu Province, the Changjiang River Delta, China	Multivariate regression and PLSR algorithms for Vis-NIR spectra have superior prediction skills than the related MIR spectra and show potential for facilitating harmful mineral assessment of soil samples.	[149]

5. Limitations of Hyperspectral Remote Sensing Data

There are several restrictions in accessing remote sensing space-borne data, but such a need is yet to be addressed. Several constraints related to data acquisition arise from climatic conditions as well as the analysis of various surface characteristics from satellite imagery [150]. The deficiency of appropriate hyperspectral space-borne sensors as well as the effective use of hyperspectral remote sensing data with lower spatial or spectral resolution bands has been neglected in cases of heavy metal pollutants monitoring and mapping [151]. Several issues are encountered in soil As monitoring in hyperspectral remote sensing, such as that the images produced by airborne or spaceborne sensors and reflectance captured by spectroradiometer are both weather-sensitive. The utility of satellite image pixels is impacted when clouds and shadows appear in it; due to this problem, images need atmospheric corrections [152]. Various researchers have observed that the reflectance recorded by remote sensors has a spectral mixing problem and offered analytical methodologies to address this issue. Thus, spectral unmixing remains difficult and requires further research [153–155].

6. Conclusions

Remote sensing techniques can be used to reduce As and other heavy metals contamination in soil, water, and rice paddy fields as well as rice grains through appropriate measures on the ground [156]. This innovative approach requires intensive research and standardisation to provide a long-term solution for reliable As estimation. The high-resolution images and the high number of bands of hyperspectral sensors might help in a detailed analysis of soil As concentration study and generate some useful information. The spectral reflectance of hyperspectral remote sensing data from various soil types can help to improve the effect of identifying specific wavelengths relevant to soil As concentration [157]. The clearest leaf reflectance reaction to plant stress is increased reflectance in the visible spectrum. Only when tension has progressed to the point of extreme leaf dehydration does infrared reflectance react consistently. The review emphasises the need for high sampling precision across a limited region, which increases interpolation accuracy while also allowing the study to examine and compare interpolations with high precision. The approach can help governments, policymakers, businesses, industries, community members, and residents to understand the optimum sampling and interpolation strategies for successfully monitoring and controlling As pollution by taking into consideration interpolation methodologies. Table 6 lists different types of spectrometers that have been used in assessing As contamination for field and laboratory purposes. Table 7 gives the detailed space-borne hyperspectral sensor specifications which have been used in the identification of many heavy metals. Soil As pollution and soil characteristics change as a result of As contamination need enhanced research, particularly in the areas of soil ecosystem restoration and long-term usage.

Table 6. Different types of spectrometer instruments for collecting spectra.

Instrument Names	Spectral Range	Spectral Resolution	Sampling Interval (Bandwidth)	Scanning Time	FOV Options	Weight	Measurement Type	Wavelength Accuracy	Study References	Website References
ASD FieldSpec 3	350–2500 nm	3 nm @ 700 nm; 10 nm @ 1400/2100 nm	1.4 nm @ 350–1050 nm; 2 nm @ 1000–2500 nm	100 ms	1.5 m fibre optic (25° field of view)	5.6 kgs (12 lbs)	Ground truthing; Remote sensing	0.5 nm	[82,109,142]	[158]
Portable visible NIR spectro-radiometer PSR-3500®	350–2500 nm	3.5 nm @350–1000 nm; 9.5 nm @1500 nm; 6.5 nm @2100 nm	1.5 nm @ 350–1000 nm; 3.8 nm @ 1500 nm; 2.5 nm@ 2100 nm	100 ms	4, 8, or 14° lenses, 25° fibre optic, diffuser, or integrating sphere	3.3 kg (7.3 lbs)	Ground truthing; Remote sensing	0.5 nm	[95]	[159]
SVC HR-1024 field spectrometer	350–2500 nm	≤3.5 nm @ 700 nm; ≤ 9.5 nm @ 1500 nm; ≤6.5 nm @ 2100 nm	≤1.5 nm @ 350–1000 nm; ≤3.8 nm @ 1000–1890 nm; ≤2.5 nm @ 1890–2500 nm	1 millisecond	4° standard, 8° and 14° optional fibre optic, 25° optional armoured fibre optic	3.3 kgs (7.3 lbs)	Ground truthing; Remote sensing		[109]	[160]
ASD FieldSpec 4 Hi-Res NG	350–2500 nm	3 nm @ 700 nm; 6 nm @ 1400/2100 nm	1.4 nm @ 350–1000 nm; 1.1 nm @ 1001–2500 nm	100 ms	1.5 m fibre optic (25° field of view). Optional narrower field of view, fibre optics available	5.44 kgs (12 lbs)	Ground truthing; remote sensing	0.5 nm	[100]	[161]
ASD FieldSpec 4 Hi-Res: High Resolution	350–2500 nm	3 nm @ 700 nm; 8 nm @ 1400/2100 nm	1.4 nm @ 350–1000 nm; 1.1 nm @ 1001–2500 nm	100 ms	1.5 m fiber optic (25° field of view). Optional narrower field of view fibre optics available	5.44 kgs (12 lbs)	Ground truthing; remote sensing	0.5 nm	[111]	[162]
ASD LabSpec 4 Hi-Res	350–2500 nm	3 nm @ 700 nm; 6 nm @ 1400/2100 nm	N.A.	100 ms	N/A	5.44 kgs (12 lbs)	Molecular structure			[163]
ASD FieldSpec Pro FR	350–2500 nm	3 nm @ 700 nm; 10 nm @ 1500 nm; 10 nm @ 2100 nm	1.4 nm @ 350–1000 nm; 2 nm @ 1000–2500 nm	100 ms	1.4 m in length with 25° full-angle cone of acceptance field of view	8 kgs (17.6 lbs)	Ground truthing; remote sensing	1 nm	[141,164]	[165]

Table 7. Details of hyperspectral space-borne sensors specifications (modified from Transon et al., 2018 [166]).

Instrument Sensor	Hyperion	Prisma	TianGong-1	HISUI	EnMAP-HYSI	SHALOM	HyspIRI	HypXIM	CHRIS	MODIS	HysIS
Satellite platform	EO-1	Prisma	Shenzhou-8	HISUI	EnMAP	IMS-II	HyspIRI	HypXIM	Proba-1	Terra and Aqua	HysIS
Spectral range (nm)	357–2576	400–2500	400–2500	400–2500	420–2450	400–2500	380–2510	400–2500	415–1050	400–1400	400–2400
Spectral bands	220	249	128	185	244	275	214	210	200	36	316
Spatial resolution (m)	30	30	30	10 (VNIR)/20 (SWIR)	30	10	30	8	18	250/500/1000	30
Spectral resolution (nm)	10	10	10 (VNIR)/23 (SWIR)	10 (VNIR)/12.5 (SWIR)	6.5 (VNIR)/10 (SWIR)	10	10	10	1.3–12		
Temporal resolution (days)	16–30	7–14		2–60	4–27	4	5–16	3–5	8	2–3	
Country agency	USA (NASA)	Italy (ASI)	China (CNSA)	Japan (JAXA)	Germany (GFZ-DLR)	Italy–Israel (ASI-ISA)	USA (NASA)	France (CNES)	UK (ESA)	USA (NASA)	India (ISRO)
Satellite mission	2000–2017	2019-present	2011–2018	2019-present	2019-present	expected launch: 2022	expected launch: 2023	expected launch: 2021	2001-present	1999-present	2018-present
Data access	*USGS-U.S. Geological Survey, 2021* [167]	*Prisma, 2019* [168]	*MSADC, 2021* [169]		*Data & Tools-EnMAP, 2012* [170]				*Earth Online, 2021* [171]	*MODIS Web, 2021* [172]	

References

1. Woolson, E.A. Arsenical pesticides. In Proceedings of the 168th Meeting of the American Chemical Society, Atlantic City, NJ, USA, 9 September 1974.
2. Mandal, B.K.; Suzuki, K.T. Arsenic round the world: A review. *Talanta* **2002**, *58*, 201–235. [CrossRef]
3. Gulledge, J.H.; O'Connor, J.T. Removal of Arsenic (V) From Water by Adsorption on Aluminum and Ferric Hydroxides. *J.-Am. Water Work. Assoc.* **1973**, *65*, 548–552. [CrossRef]
4. Kabata-Pendias, A.; Pendias, H. *Trace Elements in Soil and Plants*; No. 631.41 K3; CRC Press: Boca Raton, FL, USA, 1984.
5. Wedepohl, K.H. Composition and abundance of common sedimentary rocks. *Handb. Geochem.* **1969**, *1*, 250–271.
6. Peterson, P.; Benson, L.M.; Zeive, R. *Arsenic and Effect of Heavy Metal Pollution on Plants*; Applied Science Publishers: London, UK, 1981; p. 299.
7. Singh, H.; Goomer, S. Arsenic-A hidden poison in water-soil-rice crop continuum. *Int. J. Sci. Technol. Res.* **2019**, *8*, 864–877.
8. Masuda, H. Arsenic cycling in the Earth's crust and hydrosphere: Interaction between naturally occurring arsenic and human activities. *Prog. Earth Planet. Sci.* **2018**, *5*, 68. [CrossRef]
9. Meharg, A.A.; Williams, P.; Adomako, E.; Lawgali, Y.Y.; Deacon, C.; Villada, A.; Cambell, R.C.J.; Sun, G.; Zhu, Y.-G.; Feldmann, J.; et al. Geographical Variation in Total and Inorganic Arsenic Content of Polished (White) Rice. *Environ. Sci. Technol.* **2009**, *43*, 1612–1617. [CrossRef] [PubMed]
10. Sohn, E. Contamination: The toxic side of rice. *Nature* **2014**, *514*, S62–S63. [CrossRef]
11. Zhu, Y.-G.; Yoshinaga, M.; Zhao, F.-J.; Rosen, B.P. Earth Abides Arsenic Biotransformations. *Annu. Rev. Earth Planet. Sci.* **2014**, *42*, 443–467. [CrossRef]
12. Srivastava, S.; Tripathi, R.D.; Dhankhera, O.P.; Upadhyay, M.K. Arsenic Transport, Metabolism and Toxicity in Plants. *Int. J. Plant Environ.* **2016**, *2*, 17–28. [CrossRef]
13. Awasthi, S.; Chauhan, R.; Srivastava, S.; Tripathi, R.D. The Journey of Arsenic from Soil to Grain in Rice. *Front. Plant Sci.* **2017**, *8*, 1007. [CrossRef]
14. Wenzel, W.W. *Arsenic: Heavy Metals in Soils: Trace Metals and Metalloids in Soils and Their Bioavailability*; Alloway, B.J., Ed.; Environmental Pollution; Springer: Dordrecht, The Netherlands, 2013; Volume 22, pp. 241–282. [CrossRef]
15. Matschullat, J. Arsenic in the geosphere—A review. *Sci. Total Environ.* **2000**, *249*, 297–312. [CrossRef]
16. Meharg, A.A.; Rahman, M. Arsenic Contamination of Bangladesh Paddy Field Soils: Implications for Rice Contribution to Arsenic Consumption. *Environ. Sci. Technol.* **2003**, *37*, 229–234. [CrossRef]
17. Abedin, J.; Cotter-Howells, J.; Meharg, A.A. Arsenic uptake and accumulation in rice (*Oryza sativa* L.) irrigated with contaminated water. *Plant Soil* **2002**, *240*, 311–319. [CrossRef]
18. Pinson, S.R.M.; Tarpley, L.; Yan, W.; Yeater, K.; Lahner, B.; Yakubova, E.; Huang, X.-Y.; Zhang, M.; Guerinot, M.L.; Salt, D.E. Worldwide Genetic Diversity for Mineral Element Concentrations in Rice Grain. *Crop. Sci.* **2015**, *55*, 294–311. [CrossRef]
19. Carbonell-Barrachina, Á.A.; Signes-Pastor, A.J.; Vázquez-Araújo, L.; Burló, F.; Gupta, B.S. Presence of arsenic in agricultural products from arsenic-endemic areas and strategies to reduce arsenic intake in rural villages. *Mol. Nutr. Food Res.* **2009**, *53*, 531–541. [CrossRef] [PubMed]
20. Lin, S.-C.; Chang, T.-K.; Huang, W.-D.; Lur, H.; Shyu, G. Accumulation of arsenic in rice plant: A study of an arsenic-contaminated site in Taiwan. *Paddy Water Environ.* **2015**, *13*, 11–18. [CrossRef]

21. Roberts, L.C.; Hug, S.J.; Dittmar, J.; Voegelin, A.; Kretzschmar, R.; Wehrli, B.; Cirpka, O.A.; Saha, G.C.; Ali, M.A.; Badruzzaman, A.B.M. Arsenic release from paddy soils during monsoon flooding. *Nat. Geosci.* **2009**, *3*, 53–59. [Cross-Ref]

22. Hossain, M. Arsenic contamination in Bangladesh—An overview. *Agric. Ecosyst. Environ.* **2006**, *113*, 1–16. [CrossRef]

23. Abedin, M.J.; Feldmann, J.; Meharg, A.A. Uptake Kinetics of Arsenic Species in Rice Plants. *Plant Physiol.* **2002**, *128*, 1120–1128. [CrossRef]

24. Brammer, H. Mitigation of arsenic contamination in irrigated paddy soils in South and South-east Asia. *Environ. Int.* **2009**, *35*, 856–863. [CrossRef]

25. Li, R.Y.; Stroud, J.; Ma, J.F.; McGrath, S.; Zhao, F.-J. Mitigation of Arsenic Accumulation in Rice with Water Management and Silicon Fertilization. *Environ. Sci. Technol.* **2009**, *43*, 3778–3783. [CrossRef] [PubMed]

26. Liu, W.J.; Zhu, Y.-G.; Hu, Y.; Williams, P.; Gault, A.G.; Meharg, A.A.; Charnock, J.M.; Smith, F.A. Arsenic Sequestration in Iron Plaque, Its Accumulation and Speciation in Mature Rice Plants (*Oryza sativa* L.). *Environ. Sci. Technol.* **2006**, *40*, 5730–5736. [CrossRef] [PubMed]

27. Xie, Z.M.; Huang, C.Y. Control of arsenic toxicity in rice plants grown on an arsenic-polluted paddy soil. *Commun. Soil Sci. Plant Anal.* **1998**, *29*, 2471–2477. [CrossRef]

28. Srivastava, P.K.; Singh, M.; Gupta, M.; Singh, N.; Kharwar, R.N.; Tripathi, R.D.; Nautiyal, C.S. Mapping of arsenic pollution with reference to paddy cultivation in the middle Indo-Gangetic Plains. *Environ. Monit. Assess.* **2015**, *187*, 198. [CrossRef] [PubMed]

29. Dittmar, J.; Voegelin, A.; Roberts, L.C.; Hug, S.J.; Saha, G.C.; Ali, M.A.; Badruzzaman, A.B.M.; Kretzschmar, R. Spatial Distribution and Temporal Variability of Arsenic in Irrigated Rice Fields in Bangladesh. 2. Paddy Soil. *Environ. Sci. Technol.* **2007**, *41*, 5967–5972. [CrossRef] [PubMed]

30. Bandaru, V.; Daughtry, C.S.; Codling, E.E.; Hansen, D.J.; White-Hansen, S.; Green, C.E. Evaluating Leaf and Canopy Reflectance of Stressed Rice Plants to Monitor Arsenic Contamination. *Int. J. Environ. Res. Public Health* **2016**, *13*, 606. [CrossRef] [PubMed]

31. Tripathi, R.D.; Srivastava, S.; Mishra, S.; Singh, N.; Tuli, R.; Gupta, D.K.; Maathuis, F.J. Arsenic hazards: Strategies for tolerance and remediation by plants. *Trends Biotechnol.* **2007**, *25*, 158–165. [CrossRef]

32. Zhao, F.-J.; McGrath, S.P.; Meharg, A.A. Arsenic as a Food Chain Contaminant: Mechanisms of Plant Uptake and Metabolism and Mitigation Strategies. *Annu. Rev. Plant Biol.* **2010**, *61*, 535–559. [CrossRef] [PubMed]

33. Dat, J.; Vandenabeele, S.; Vranová, E.; Van Montagu, M.; Inzé, D.; Van Breusegem, F. Dual action of the active oxygen species during plant stress responses. *Cell. Mol. Life Sci.* **2000**, *57*, 779–795. [CrossRef]

34. Whitaker, J.; Ainsworth, G.; Meharg, A. Copper- and arsenate-induced oxidative stress in Holcus lanatus L. clones with differential sensitivity. *Plant Cell Environ.* **2001**, *24*, 713–722. [CrossRef]

35. Flora, S.J. Arsenic-induced oxidative stress and its reversibility following combined administration of n-acetylcysteine and meso 2, 3–dimercaptosuccinic acid in rats. *Clin. Exp. Pharmacol. Physiol.* **1999**, *26*, 865–869. [CrossRef] [PubMed]

36. Choudhury, B.; Chowdhury, S.; Biswas, A.K. Regulation of growth and metabolism in rice (*Oryza sativa* L.) by arsenic and its possible reversal by phosphate. *J. Plant Interact.* **2011**, *6*, 15–24. [CrossRef]

37. Azizur Rahman, M.; Hasegawa, H.; Mahfuzur Rahman, M.; Nazrul Islam, M.; Majid Miah, M.A.; Tasmen, A. Effect of arsenic on photosynthesis, growth and yield of five widely cultivated rice (*Oryza sativa* L.) varieties in Bangladesh. *Chemosphere* **2007**, *67*, 1072–1079. [CrossRef]

38. Shaibur, M.R.; Kitajima, N.; Sugawara, R.; Kondo, T.; Huq, S.M.I.; Kawai, S. Physiological and mineralogical properties of arsenic-induced chlorosis in rice seedlings grown hydroponically. *Soil Sci. Plant Nutr.* **2006**, *52*, 691–700. [CrossRef]

39. *Feed Additive Compendium*; The Miller Publishing Company: Minneapolis, MN, USA, 1975; Volume 13, p. 330.

40. Miteva, E. Accumulation and effect of arsenic on tomatoes. *Commun. Soil Sci. Plant Anal.* **2002**, *33*, 1917–1926. [CrossRef]

41. Rahman, M.A.; Hasegawa, H.; Rahman, M.M.; Rahman, M.A.; Miah, M.A.M. Accumulation of arsenic in tissues of rice plant (Oryza sativa L.) and its distribution in fractions of rice grain. *Chemosphere* **2007**, *69*, 942–948. [CrossRef]

42. Rensing, C.; Rosen, B. Biogeocycles for redox-active metal(loids): As, Cu, Mn and Se. In *Encyclopedia of Microbiology*; Schaechter, M., Ed.; Elsevier: Oxford, UK, 2009; pp. 205–219.

43. Colmer, T.D.; Cox, M.C.H.; Voesenek, L. Root aeration in rice (*Oryza sativa*): Evaluation of oxygen, carbon dioxide, and ethylene as possible regulators of root acclimatizations. *New Phytol.* **2006**, *170*, 767–777. [CrossRef]

44. Wikipedia. Rhizosphere. 2021. Available online: https://en.wikipedia.org/wiki/Rhizosphere#:~{}:text=The%20rhizosphere%20is%20the%20narrow,known%20as%20the%20root%20microbiome (accessed on 9 April 2021).

45. Santra, S.C.; Samal, A.C.; Bhattacharya, P.; Banerjee, S.; Biswas, A.; Majumdar, J. Arsenic in Foodchain and Community Health Risk: A Study in Gangetic West Bengal. *Procedia Environ. Sci.* **2013**, *18*, 2–13. [CrossRef]

46. Chowdhury, U.K.; Rahman, M.M.; Mandal, B.K.; Paul, K.; Lodh, D.; Biswas, B.K.; Chakraborti, D. Groundwater arsenic contamination and human suffering in West Bengal, India and Bangladesh. *Environ. Sci.* **2001**, *8*, 393–415.

47. Roychowdhury, T.; Uchino, T.; Tokunaga, H.; Ando, M. Survey of arsenic in food composites from an arsenic-affected area of West Bengal, India. *Food Chem. Toxicol.* **2002**, *40*, 1611–1621. [CrossRef]

48. Alam, M.; Snow, E.; Tanaka, A. Arsenic and heavy metal contamination of vegetables grown in Samta village, Bangladesh. *Sci. Total Environ.* **2003**, *308*, 83–96. [CrossRef]

49. Farid, A.T.M.; Roy, K.C.; Hossain, K.M.; Sen, R. A study of arsenic contaminated irrigation water and it's carried over effect on vegetable. Fate of arsenic in the environment. *Dhaka Bangladesh Univ. Eng. Technol.* **2003**, 113–121. Available online: http://citeseerx.ist.psu.edu/viewdoc/download?doi=10.1.1.495.8268&rep=rep1&type=pdf (accessed on 13 May 2021).

50. Das, H.; Mitra, A.; Sengupta, P.; Hossain, A.; Islam, F.; Rabbani, G. Arsenic concentrations in rice, vegetables, and fish in Bangladesh: A preliminary study. *Environ. Int.* **2004**, *30*, 383–387. [CrossRef]

51. Norra, S.; Berner, Z.A.; Agarwala, P.; Wagner, F.; Chandrasekharam, D.; Stüben, D. Impact of irrigation with As rich groundwater on soil and crops: A geochemical case study in West Bengal Delta Plain, India. *Appl. Geochem.* **2005**, *20*, 1890–1906. [CrossRef]

52. Huang, R.-Q.; Gao, S.-F.; Wang, W.-L.; Staunton, S.; Wang, G. Soil arsenic availability and the transfer of soil arsenic to crops in suburban areas in Fujian Province, southeast China. *Sci. Total Environ.* **2006**, *368*, 531–541. [CrossRef]

53. Dahal, B.; Fuerhacker, M.; Mentler, A.; Karki, K.; Shrestha, R.; Blum, W. Arsenic contamination of soils and agricultural plants through irrigation water in Nepal. *Environ. Pollut.* **2008**, *155*, 157–163. [CrossRef]

54. Bhattacharya, P.; Samal, A.C.; Majumdar, J.; Santra, S.C. Transfer of arsenic from groundwater and paddy soil to rice plant (*Oryza sativa* L.): A micro level study in West Bengal, India. *World J. Agric. Sci.* **2009**, *5*, 425–431.

55. Bhattacharya, P.; Samal, A.C.; Majumdar, J.; Santra, S. Arsenic Contamination in Rice, Wheat, Pulses, and Vegetables: A Study in an Arsenic Affected Area of West Bengal, India. *Water Air Soil Pollut.* **2010**, *213*, 3–13. [CrossRef]

56. Singh, S.K.; Ghosh, A.K. Entry of arsenic into food material-a case study. *World Appl. Sci. J.* **2011**, *13*, 385–390.

57. Samal, A.C.; Kar, S.; Bhattacharya, P.; Santra, S. Human exposure to arsenic through foodstuffs cultivated using arsenic contaminated groundwater in areas of West Bengal, India. *J. Environ. Sci. Health Part A* **2011**, *46*, 1259–1265. [CrossRef]

58. Halder, D.; Bhowmick, S.; Biswas, A.; Chatterjee, D.; Nriagu, J.; Mazumder, D.N.G.; Šlejkovec, Z.; Jacks, G.; Bhattacharya, P. Risk of Arsenic Exposure from Drinking Water and Dietary Components: Implications for Risk Management in Rural Bengal. *Environ. Sci. Technol.* **2012**, *47*, 1120–1127. [CrossRef] [PubMed]

59. Takebe, M.; Yoneyama, T.; Inada, K.; Murakami, T. Spectral reflectance ratio of rice canopy for estimating crop nitrogen status. *Plant Soil* **1990**, *122*, 295–297. [CrossRef]

60. Kemper, T.; Sommer, S. Estimate of Heavy Metal Contamination in Soils after a Mining Accident Using Reflectance Spectroscopy. *Environ. Sci. Technol.* **2002**, *36*, 2742–2747. [CrossRef] [PubMed]

61. Choe, E.; Van Der Meer, F.; Van Ruitenbeek, F.; Van Der Werff, H.; De Smeth, B.; Kim, K.-W. Mapping of heavy metal pollution in stream sediments using combined geochemistry, field spectroscopy, and hyperspectral remote sensing: A case study of the Rodalquilar mining area, SE Spain. *Remote Sens. Environ.* **2008**, *112*, 3222–3233. [CrossRef]

62. Shi, T.; Chen, Y.; Liu, Y.; Wu, G. Visible and near-infrared reflectance spectroscopy—An alternative for monitoring soil contamination by heavy metals. *J. Hazard. Mater.* **2014**, *265*, 166–176. [CrossRef]

63. Wu, Y.Z.; Chen, J.; Ji, J.F.; Tian, Q.J.; Wu, X.M. Feasibility of Reflectance Spectroscopy for the Assessment of Soil Mercury Contamination. *Environ. Sci. Technol.* **2005**, *39*, 873–878. [CrossRef]

64. Wu, Y.; Zhang, X.; Liao, Q.; Ji, J. Can contaminant elements in soils be assessed by remote sensing technology. *Soil Sci.* **2011**, *176*, 196–205. [CrossRef]

65. Clevers, J. Application of the WDVI in estimating LAI at the generative stage of barley. *ISPRS J. Photogramm. Remote Sens.* **1991**, *46*, 37–47. [CrossRef]

66. Schaepman, M.E.; Koetz, B.; Schaepman-Strub, G.; Itten, K.I. Spectrodirectional remote sensing for the improved estimation of biophysical and -chemical variables: Two case studies. *Int. J. Appl. Earth Obs. Geoinf.* **2005**, *6*, 271–282. [CrossRef]

67. Imanishi, J.; Nakayama, A.; Suzuki, Y.; Imanishi, A.; Ueda, N.; Morimoto, Y.; Yoneda, M. Nondestructive determination of leaf chlorophyll content in two flowering cherries using reflectance and absorptance spectra. *Landsc. Ecol. Eng.* **2010**, *6*, 219–234. [CrossRef]

68. Bannari, A.; Khurshid, K.S.; Staenz, K.; Schwarz, J.W. A Comparison of Hyperspectral Chlorophyll Indices for Wheat Crop Chlorophyll Content Estimation Using Laboratory Reflectance Measurements. *IEEE Trans. Geosci. Remote Sens.* **2007**, *45*, 3063–3074. [CrossRef]

69. Cheng, T.; Rivard, B.; Sanchez-Azofeifa, A. Spectroscopic determination of leaf water content using continuous wavelet analysis. *Remote Sens. Environ.* **2011**, *115*, 659–670. [CrossRef]

70. Danson, F.M.; Steven, M.D.; Malthus, T.J.; Clark, J.A. High-spectral resolution data for determining leaf water content. *Int. J. Remote Sens.* **1992**, *13*, 461–470. [CrossRef]

71. Saha, A.; Patil, M.; Goyal, V.C.; Rathore, D.S. Assessment and Impact of Soil Moisture Index in Agricultural Drought Estimation Using Remote Sensing and GIS Techniques. *Proceedings* **2019**, *7*, 2. [CrossRef]

72. Dunagan, S.C.; Gilmore, M.S.; Varekamp, J.C. Effects of mercury on visible/near-infrared reflectance spectra of mustard spinach plants (Brassica rapa P.). *Environ. Pollut.* **2007**, *148*, 301–311. [CrossRef] [PubMed]

73. Carter, G.A. Responses of leaf spectral reflectance to plant stress. *Am. J. Bot.* **1993**, *80*, 239–243. [CrossRef]

74. Liu, M.; Liu, X.; Ding, W.; Wu, L. Monitoring stress levels on rice with heavy metal pollution from hyperspectral reflectance data using wavelet-fractal analysis. *Int. J. Appl. Earth Obs. Geoinf.* **2011**, *13*, 246–255. [CrossRef]

75. Meggio, F.; Zarco-Tejada, P.; Núñez, L.; Sepulcre-Cantó, G.; González, M.; Martin, P. Grape quality assessment in vineyards affected by iron deficiency chlorosis using narrow-band physiological remote sensing indices. *Remote Sens. Environ.* **2010**, *114*, 1968–1986. [CrossRef]

76.   Bandaru, V.; Hansen, D.J.; Codling, E.E.; Daughtry, C.; White-Hansen, S.; Green, C.E. Quantifying arsenic-induced morphological changes in spinach leaves: Implications for remote sensing. *Int. J. Remote Sens.* **2010**, *31*, 4163–4177. [CrossRef]

77.   Carter, G.A.; Knapp, A.K. Leaf optical properties in higher plants: Linking spectral characteristics to stress and chlorophyll concentration. *Am. J. Bot.* **2001**, *88*, 677–684. [CrossRef]

78.   Yang, C.-M.; Cheng, C.-H.; Chen, R.-K. Changes in Spectral Characteristics of Rice Canopy Infested with Brown Planthopper and Leaffolder. *Crop Sci.* **2007**, *47*, 329–335. [CrossRef]

79.   Shi, T.; Liu, H.; Wang, J.; Chen, Y.; Fei, T.; Wu, G. Monitoring Arsenic Contamination in Agricultural Soils with Reflectance Spectroscopy of Rice Plants. *Environ. Sci. Technol.* **2014**, *48*, 6264–6272. [CrossRef] [PubMed]

80.   Daughtry, C.S.T.; Walthall, C.L.; Kim, M.S.; De Colstoun, E.B.; McMurtrey, J.E., III. Estimating Corn Leaf Chlorophyll Concentration from Leaf and Canopy Reflectance. *Remote. Sens. Environ.* **2000**, *74*, 229–239. [CrossRef]

81.   Eitel, J.U.H.; Long, D.S.; Gessler, P.E.; Hunt, E.R. Combined Spectral Index to Improve Ground-Based Estimates of Nitrogen Status in Dryland Wheat. *Agron. J.* **2008**, *100*, 1694–1702. [CrossRef]

82.   Lv, J.; Liu, X. Predicting arsenic concentration in rice plants from hyperspectral data using random forests. In *Advances in Multimedia, Software Engineering and Computing*; Springer: Berlin/Heidelberg, Germany, 2011; Volume 1, pp. 601–606. [CrossRef]

83.   Breiman, L. Random forests. *Mach. Learn.* **2001**, *45*, 5–32. [CrossRef]

84.   Wu, Y.; Chen, J.; Wu, X.; Tian, Q.; Ji, J.; Qin, Z. Possibilities of reflectance spectroscopy for the assessment of contaminant elements in suburban soils. *Appl. Geochem.* **2005**, *20*, 1051–1059. [CrossRef]

85.   Zhou, W.; Zhang, J.; Zou, M.; Liu, X.; Du, X.; Wang, Q.; Liu, Y.; Liu, Y.; Li, J. Feasibility of Using Rice Leaves Hyperspectral Data to Estimate CaCl2-extractable Concentrations of Heavy Metals in Agricultural Soil. *Sci. Rep.* **2019**, *9*, 16084. [CrossRef]

86.   Chapin, F.S. Iii Integrated Responses of Plants to Stress. *Bioscience* **1991**, *41*, 29–36. [CrossRef]

87.   Brown, D.J.; Shepherd, K.D.; Walsh, M.G.; Mays, M.D.; Reinsch, T.G. Global soil characterization with VNIR diffuse reflectance spectroscopy. *Geoderma* **2005**, *132*, 273–290. [CrossRef]

88.   Barnes, R.J.; Dhanoa, M.S.; Lister, S.J. Standard Normal Variate Transformation and De-Trending of Near-Infrared Diffuse Reflectance Spectra. *Appl. Spectrosc.* **1989**, *43*, 772–777. [CrossRef]

89.   Chu, X.; Yuan, H.; Lu, W. Progress and application of spectral data pretreatment and wavelength selection methods in NIR analytical technique. *Prog. Chem.* **2004**, *16*, 528.

90.   Candolfi, A.; De Maesschalck, R.; Jouan-Rimbaud, D.; Hailey, P.; Massart, D. The influence of data pre-processing in the pattern recognition of excipients near-infrared spectra. *J. Pharm. Biomed. Anal.* **1999**, *21*, 115–132. [CrossRef] [PubMed]

91.   Rinnan, Å.; van den Berg, F.; Engelsen, S.B. Review of the most common pre-processing techniques for near-infrared spectra. *TrAC Trends Anal. Chem.* **2009**, *28*, 1201–1222. [CrossRef]

92.   Liu, Y.; Liu, Y.; Chen, Y.; Zhang, Y.; Shi, T.; Wang, J.; Hong, Y.; Fei, T. The Influence of Spectral Pretreatment on the Selection of Representative Calibration Samples for Soil Organic Matter Estimation Using Vis-NIR Reflectance Spectroscopy. *Remote Sens.* **2019**, *11*, 450. [CrossRef]

93.   Clark, R.N.; Roush, T.L. Reflectance spectroscopy: Quantitative analysis techniques for remote sensing applications. *J. Geophys. Res. Earth Surf.* **1984**, *89*, 6329–6340. [CrossRef]

94.   Hook, J. Smoothing non-smooth systems with low-pass filters. *Phys. D Nonlinear Phenom.* **2014**, *269*, 76–85. [CrossRef]

95.   Chakraborty, S.; Li, B.; Deb, S.; Paul, S.; Weindorf, D.C.; Das, B.S. Predicting soil arsenic pools by visible near infrared diffuse reflectance spectroscopy. *Geoderma* **2017**, *296*, 30–37. [CrossRef]

96.   Continuum Removal. 2020. Available online: https://www.l3harrisgeospatial.com/docs/continuumremoval.html (accessed on 20 May 2021).

97.   Chakraborty, S.; Das, B.S.; Ali, N.; Li, B.; Sarathjith, M.; Majumdar, K.; Ray, D. Rapid estimation of compost enzymatic activity by spectral analysis method combined with machine learning. *Waste Manag.* **2014**, *34*, 623–631. [CrossRef]

98.   R: The R Project for Statistical Computing. Available online: https://www.r-project.org/ (accessed on 10 May 2021).

99.   Luo, J.; Ying, K.; He, P.; Bai, J. Properties of Savitzky–Golay digital differentiators. *Digit. Signal Process.* **2005**, *15*, 122–136. [CrossRef]

100.   Han, L.; Chen, R.; Zhu, H.; Zhao, Y.; Liu, Z.; Huo, H. Estimating Soil Arsenic Content with Visible and Near-Infrared Hyperspectral Reflectance. *Sustainability* **2020**, *12*, 1476. [CrossRef]

101.   Curran, P.J.; Dungan, J.L.; Peterson, D.L. Estimating the foliar biochemical concentration of leaves with reflectance spectrometry: Testing the Kokaly and Clark methodologies. *Remote Sens. Environ.* **2001**, *76*, 349–359. [CrossRef]

102.   Tan, K.; Ye, Y.-Y.; Du, P.-J.; Zhang, Q.-Q. Estimation of heavy metal concentrations in reclaimed mining soils using reflectance spectroscopy. *Guang Pu Xue Yu Guang Pu Fen Xi Guang Pu* **2014**, *34*, 3317–3322. [CrossRef]

103.   Zhao, L.; Hu, Y.-M.; Zhou, W.; Liu, Z.-H.; Pan, Y.-C.; Shi, Z.; Wang, L.; Wang, G.-X. Estimation Methods for Soil Mercury Content Using Hyperspectral Remote Sensing. *Sustainability* **2018**, *10*, 2474. [CrossRef]

104.   Wu, Y.; Chen, J.; Ji, J.; Gong, P.; Liao, Q.; Tian, Q.; Ma, H. A Mechanism Study of Reflectance Spectroscopy for Investigating Heavy Metals in Soils. *Soil Sci. Soc. Am. J.* **2007**, *71*, 918–926. [CrossRef]

105.   Choe, E.; Kim, K.-W.; Bang, S.; Yoon, I.-H.; Lee, K.-Y. Qualitative analysis and mapping of heavy metals in an abandoned Au–Ag mine area using NIR spectroscopy. *Environ. Earth Sci.* **2009**, *58*, 477–482. [CrossRef]

106.   Ji, J.; Song, Y.; Yuan, X.; Yang, Z. Diffuse reflectance spectroscopy study of heavy metals in agricultural soils of the Changjiang River Delta, China. In Proceedings of the 19th World Congress of Soil Science, Brisbane, Australia, 1–6 August 2010.

107. Tan, K.; Ye, Y.; Cao, Q.; Du, P.; Dong, J. Estimation of Arsenic Contamination in Reclaimed Agricultural Soils Using Reflectance Spectroscopy and ANFIS Model. *IEEE J. Sel. Top. Appl. Earth Obs. Remote Sens.* **2014**, *7*, 2540–2546. [CrossRef]

108. Gholizadeh, A.; Boruvka, L.; Vašát, R.; Saberioon, M.; Klement, A.; Kratina, J.; Tejnecký, V.; Drábek, O. Estimation of Potentially Toxic Elements Contamination in Anthropogenic Soils on a Brown Coal Mining Dumpsite by Reflectance Spectroscopy: A Case Study. *PLoS ONE* **2015**, *10*, e0117457. [CrossRef]

109. Wei, L.; Yuan, Z.; Yu, M.; Huang, C.; Cao, L. Estimation of Arsenic Content in Soil Based on Laboratory and Field Reflectance Spectroscopy. *Sensors* **2019**, *19*, 3904. [CrossRef]

110. Tao, C.; Wang, Y.; Cui, W.; Zou, B.; Zou, Z.; Tu, Y. A transferable spectroscopic diagnosis model for predicting arsenic contamination in soil. *Sci. Total Environ.* **2019**, *669*, 964–972. [CrossRef]

111. Pyo, J.; Hong, S.M.; Kwon, Y.S.; Kim, M.S.; Cho, K.H. Estimation of heavy metals using deep neural network with visible and infrared spectroscopy of soil. *Sci. Total Environ.* **2020**, *741*, 140162. [CrossRef]

112. Wei, L.; Pu, H.; Wang, Z.; Yuan, Z.; Yan, X.; Cao, L. Estimation of Soil Arsenic Content with Hyperspectral Remote Sensing. *Sensors* **2020**, *20*, 4056. [CrossRef] [PubMed]

113. Kukier, U.; Chaney, R.L. Growing rice grain with controlled cadmium concentrations. *J. Plant Nutr.* **2002**, *25*, 1793–1820. [CrossRef]

114. Rouse, J.W.; Haas, R.H.; Schell, J.A.; Deering, D.W.; Harlan, J.C. Monitoring the Vernal Advancement and Retrogradation (Green Wave Effect) of Natural Vegetation. NASA/GSFC Type III Final Report, Greenbelt, Md. 1974; 371p. Available online: http://citeseerx.ist.psu.edu/viewdoc/download?doi=10.1.1.464.7884&rep=rep1&type=pdf (accessed on 23 May 2021).

115. Rondeaux, G.; Steven, M.; Baret, F. Optimization of soil-adjusted vegetation indices. *Remote Sens. Environ.* **1996**, *55*, 95–107. [CrossRef]

116. SAS Institute Inc. *SAS*; SAS Institute Inc.: Cary, NC, USA, 2002.

117. Smith, K.L.; Steven, M.D.; Colls, J.J. Use of hyperspectral derivative ratios in the red-edge region to identify plant stress responses to gas leaks. *Remote Sens. Environ.* **2004**, *92*, 207–217. [CrossRef]

118. Fan, S.; Zhang, B.; Li, J.; Liu, C.; Huang, W.; Tian, X. Prediction of soluble solids content of apple using the combination of spectra and textural features of hyperspectral reflectance imaging data. *Postharvest Biol. Technol.* **2016**, *121*, 51–61. [CrossRef]

119. Zheng, K.; Li, Q.; Wang, J.; Geng, J.; Cao, P.; Sui, T.; Wang, X.; Du, Y. Stability competitive adaptive reweighted sampling (SCARS) and its applications to multivariate calibration of NIR spectra. *Chemom. Intell. Lab. Syst.* **2012**, *112*, 48–54. [CrossRef]

120. Wang, S.; Chen, Y.; Wang, M.; Zhao, Y.; Li, J. SPA-Based Methods for the Quantitative Estimation of the Soil Salt Content in Saline-Alkali Land from Field Spectroscopy Data: A Case Study from the Yellow River Irrigation Regions. *Remote Sens.* **2019**, *11*, 967. [CrossRef]

121. Gholizadeh, A.; Žižala, D.; Saberioon, M.; Borůvka, L. Soil organic carbon and texture retrieving and mapping using proximal, airborne and Sentinel-2 spectral imaging. *Remote Sens. Environ.* **2018**, *218*, 89–103. [CrossRef]

122. Yang, L.I.; Haidong, L.I.; Weisheng, S. Prediction and Ecological risk assessment of heavy metals in soil based on neural network. *Res. Environ. Yangtze Basin* **2017**, *26*, 591–597.

123. Zhang, S.; Shen, Q.; Nie, C.; Huang, Y.; Wang, J.; Hu, Q.; Ding, X.; Zhou, Y.; Chen, Y. Hyperspectral inversion of heavy metal content in reclaimed soil from a mining wasteland based on different spectral transformation and modeling methods. *Spectrochim. Acta Part A Mol. Biomol. Spectrosc.* **2019**, *211*, 393–400. [CrossRef]

124. Ramoelo, A.; Skidmore, A.; Cho, M.; Mathieu, R.; Heitkönig, I.; Dudeni-Tlhone, N.; Schlerf, M.; Prins, H. Non-linear partial least square regression increases the estimation accuracy of grass nitrogen and phosphorus using in situ hyperspectral and environmental data. *ISPRS J. Photogramm. Remote Sens.* **2013**, *82*, 27–40. [CrossRef]

125. Clavaud, M.; Roggo, Y.; Dégardin, K.; Sacré, P.-Y.; Hubert, P.; Ziemons, E. Global regression model for moisture content determination using near-infrared spectroscopy. *Eur. J. Pharm. Biopharm.* **2017**, *119*, 343–352. [CrossRef] [PubMed]

126. Mackay, D.J.C. Bayesian Interpolation. *Neural Comput.* **1992**, *4*, 415–447. [CrossRef]

127. Walker, S.G.; Page, C.J. Generalized ridge regression and a generalization of theCPstatistic. *J. Appl. Stat.* **2001**, *28*, 911–922. [CrossRef]

128. Avron, H.; Clarkson, K.L.; Woodruff, D.P. Faster Kernel Ridge Regression Using Sketching and Preconditioning. *SIAM J. Matrix Anal. Appl.* **2017**, *38*, 1116–1138. [CrossRef]

129. Tong, H.; Chen, D.-R.; Yang, F. Support vector machines regression with unbounded sampling. *Appl. Anal.* **2018**, *98*, 1626–1635. [CrossRef]

130. Tan, K.; Wang, H.; Zhang, Q.; Jia, X. An improved estimation model for soil heavy metal(loid) concentration retrieval in mining areas using reflectance spectroscopy. *J. Soils Sediments* **2018**, *18*, 2008–2022. [CrossRef]

131. Chen, T.; Guestrin, C. Xgboost: A scalable tree boosting system. In Proceedings of the 22nd Acm Sigkdd International Conference on Knowledge Discovery and Data Mining, San Francisco, CA, USA, 13–17 August 2016; pp. 785–794. [CrossRef]

132. Ishwaran, H.; Lu, M. Standard errors and confidence intervals for variable importance in random forest regression, classification, and survival. *Stat. Med.* **2019**, *38*, 558–582. [CrossRef]

133. Singh, B.; Sihag, P.; Singh, K. Modelling of impact of water quality on infiltration rate of soil by random forest regression. *Model. Earth Syst. Environ.* **2017**, *3*, 999–1004. [CrossRef]

134. Yun, Y.-H.; Wang, W.-T.; Tan, M.-L.; Liang, Y.-Z.; Li, H.-D.; Cao, D.-S.; Lu, H.-M.; Xu, Q.-S. A strategy that iteratively retains informative variables for selecting optimal variable subset in multivariate calibration. *Anal. Chim. Acta* **2014**, *807*, 36–43. [CrossRef]

135. Zhang, H.; Wang, H.; Dai, Z.; Chen, M.-S.; Yuan, Z. Improving accuracy for cancer classification with a new algorithm for genes selection. *BMC Bioinform.* **2012**, *13*, 298. [CrossRef] [PubMed]

136. Ren, H.-Y.; Zhuang, D.-F.; Singh, A.; Pan, J.-J.; Qiu, D.-S.; Shi, R.-H. Estimation of As and Cu Contamination in Agricultural Soils Around a Mining Area by Reflectance Spectroscopy: A Case Study. *Pedosphere* **2009**, *19*, 719–726. [CrossRef]

137. Wang, J.; Cui, L.; Gao, W.; Shi, T.; Chen, Y.; Gao, Y. Prediction of low heavy metal concentrations in agricultural soils using visible and near-infrared reflectance spectroscopy. *Geoderma* **2014**, *216*, 1–9. [CrossRef]

138. Mitchell, A. *Modeling Suitability, Movement, and Interaction*; Esri Press: Tokyo, Japan, 2012.

139. Weerasiri, T.; Wirojanagud, W.; Srisatit, T. Assessment of Potential Location of High Arsenic Contamination Using Fuzzy Overlay and Spatial Anisotropy Approach in Iron Mine Surrounding Area. *Sci. World J.* **2014**, *2014*, 905362. [CrossRef] [PubMed]

140. Tian, Y.; Yao, X.; Yang, J.; Cao, W.; Hannaway, D.; Zhu, Y. Assessing newly developed and published vegetation indices for estimating rice leaf nitrogen concentration with ground- and space-based hyperspectral reflectance. *Field Crop. Res.* **2011**, *120*, 299–310. [CrossRef]

141. Li, X.; Liu, X.; Liu, M.; Wang, C.; Xia, X. A hyperspectral index sensitive to subtle changes in the canopy chlorophyll content under arsenic stress. *Int. J. Appl. Earth Obs. Geoinf.* **2015**, *36*, 41–53. [CrossRef]

142. Shi, T.; Liu, H.; Chen, Y.; Wang, J.; Wu, G. Estimation of arsenic in agricultural soils using hyperspectral vegetation indices of rice. *J. Hazard. Mater.* **2016**, *308*, 243–252. [CrossRef]

143. Barton, C.V.M. Advances in remote sensing of plant stress. *Plant Soil* **2012**, *354*, 41–44. [CrossRef]

144. Clevers, J.G.P.W.; Kooistra, L.; Salas, E.A.L. Study of heavy metal contamination in river floodplains using the red-edge position in spectroscopic data. *Int. J. Remote Sens.* **2004**, *25*, 3883–3895. [CrossRef]

145. Shi, T.; Wang, J.; Liu, H.; Wu, G. Estimating leaf nitrogen concentration in heterogeneous crop plants from hyperspectral reflectance. *Int. J. Remote Sens.* **2015**, *36*, 4652–4667. [CrossRef]

146. Muller, G. Index of geoaccumulation in sediments of the Rhine River. *Geojournal* **1969**, *2*, 108–118.

147. Loska, K.; Wiechuła, D.; Korus, I. Metal contamination of farming soils affected by industry. *Environ. Int.* **2004**, *30*, 159–165. [CrossRef]

148. Gamon, J.A.; Peñuelas, J.; Field, C.B. A narrow-waveband spectral index that tracks diurnal changes in photosynthetic efficiency. *Remote Sens. Environ.* **1992**, *41*, 35–44. [CrossRef]

149. Song, Y.; Li, F.; Yang, Z.; Ayoko, G.; Frost, R.L.; Ji, J. Diffuse reflectance spectroscopy for monitoring potentially toxic elements in the agricultural soils of Changjiang River Delta, China. *Appl. Clay Sci.* **2012**, *64*, 75–83. [CrossRef]

150. Zhang, D.; Zhou, G. Estimation of Soil Moisture from Optical and Thermal Remote Sensing: A Review. *Sensors* **2016**, *16*, 1308. [CrossRef]

151. Gholizadeh, A.; Saberioon, M.; Ben-Dor, E.; Borůvka, L. Monitoring of selected soil contaminants using proximal and remote sensing techniques: Background, state-of-the-art and future perspectives. *Crit. Rev. Environ. Sci. Technol.* **2018**, *48*, 243–278. [CrossRef]

152. Abdellatif, B.; Lecerf, R.; Mercier, G.; Hubert-Moy, L. Preprocessing of Low-Resolution Time Series Contaminated by Clouds and Shadows. *IEEE Trans. Geosci. Remote Sens.* **2008**, *46*, 2083–2096. [CrossRef]

153. Somers, B.; Asner, G.P.; Tits, L.; Coppin, P. Endmember variability in Spectral Mixture Analysis: A review. *Remote Sens. Environ.* **2011**, *115*, 1603–1616. [CrossRef]

154. Heylen, R.; Parente, M.; Gader, P. A Review of Nonlinear Hyperspectral Unmixing Methods. *IEEE J. Sel. Top. Appl. Earth Obs. Remote Sens.* **2014**, *7*, 1844–1868. [CrossRef]

155. Saha, A.; Garg, P.K.; Patil, M. The effect of contaminated snow reflectance using hyperspectral remote sensing—A review. *Int. J. Image Data Fusion* **2018**, *10*, 107–130. [CrossRef]

156. Wang, F.; Gao, J.; Zha, Y. Hyperspectral sensing of heavy metals in soil and vegetation: Feasibility and challenges. ISPRS J. Photogramm. *Remote Sens.* **2018**, *136*, 73–84. [CrossRef]

157. El-Hendawy, S.E.; Al-Suhaibani, N.A.; Hassan, W.; Dewir, Y.H.; Elsayed, S.; Al-Ashkar, I.; Abdella, K.A.; Schmidhalter, U. Evaluation of wavelengths and spectral reflectance indices for high-throughput assessment of growth, water relations and ion contents of wheat irrigated with saline water. *Agric. Water Manag.* **2019**, *212*, 358–377. [CrossRef]

158. FieldSpec 3 Spectroradiometer. 2021. Available online: http://www.samwoosc.co.kr/fieldspec3.html (accessed on 23 May 2021).

159. PSR-3500-Spectral Evolution. 2017. Available online: https://spectralevolution.s3.us-east-2.amazonaws.com/assets/20171103185526/Remote_Sensing_GRSG_B.pdf (accessed on 23 May 2021).

160. SVC HR-1024. 2016. Available online: https://www.spectravista.com/wp-content/uploads/2016/07/SVC-HR-1024-Specs.pdf (accessed on 23 May 2021).

161. ASD FieldSpec 4 Hi-Res NG Spectroradiometer. 2021. Available online: https://www.malvernpanalytical.com/en/products/product-range/asd-range/fieldspec-range/fieldspec-4-hi-res-ng-spectroradiometer (accessed on 23 May 2021).

162. ASD FieldSpec 4 Hi-Res: High Resolution Spectroradiometer. 2021. Available online: https://www.malvernpanalytical.com/en/products/product-range/asd-range/fieldspec-range/fieldspec4-hi-res-high-resolution-spectroradiometer (accessed on 23 May 2021).

163. ASD LabSpec 4 Hi-Res Analytical Instrument. 2013. Available online: https://www.malvernpanalytical.com/en/products/product-range/asd-range/labspec-range/labspec-4-hi-res-analytical-instrument (accessed on 23 May 2021).

164. Gholizadeh, A.; Saberioon, M.; Carmon, N.; Boruvka, L.; Ben-Dor, E. Examining the Performance of PARACUDA-II Data-Mining Engine versus Selected Techniques to Model Soil Carbon from Reflectance Spectra. *Remote Sens.* **2018**, *10*, 1172. [CrossRef]
165. FieldSpec Pro FR Portable Spectroradiometer. 2021. Available online: https://www.laboratorynetwork.com/doc/fieldspec-pro-fr-portable-spectroradiometer-0001 (accessed on 23 May 2021).
166. Transon, J.; D'Andrimont, R.; Maugnard, A.; Defourny, P. Survey of Hyperspectral Earth Observation Applications from Space in the Sentinel-2 Context. *Remote Sens.* **2018**, *10*, 157. [CrossRef]
167. USGS (United States Geological Survey). Available online: https://earthexplorer.usgs.gov (accessed on 10 June 2017).
168. Prisma. 2019. Available online: http://www.prisma-i.it/index.php/en/ (accessed on 13 May 2021).
169. MSADC. 2021. Available online: http://msadc.cn/en/sjfw/tg2sj/ (accessed on 13 May 2021).
170. Data & Tools–EnMAP. 2012. Available online: https://www.enmap.org/data_tools/ (accessed on 13 May 2021).
171. Earth Online. 2021. Available online: https://earth.esa.int/eogateway/ (accessed on 13 May 2021).
172. MODIS Web. 2021. Available online: https://modis.gsfc.nasa.gov/ (accessed on 13 May 2021).